

1 **Design principles to tailor Hsp104 therapeutics**

2
3 JiaBei Lin¹, Peter J. Carman^{1,2}, Craig W. Gambogi^{1,2}, Nathan M. Kendersky^{1,3}, Edward
4 Chuang^{1,3}, Stephanie N. Gates^{4,6}, Adam L. Yokom^{4,6}, Alexandria N. Rizo⁴, Daniel R.
5 Southworth⁵, and James Shorter^{1,2,3*}.

6
7 ¹Department of Biochemistry and Biophysics, ²Biochemistry and Molecular Biophysics Graduate
8 Group, ³Pharmacology Graduate Group Perelman School of Medicine, University of
9 Pennsylvania, Philadelphia, PA 19104. U.S.A.

10
11 ⁴Graduate Program in Chemical Biology, University of Michigan, Ann Arbor, MI 48109. U.S.A.

12
13 ⁵Department of Biochemistry and Biophysics and the Institute for Neurodegenerative Diseases,
14 University of California San Francisco, San Francisco, CA 94158. U.S.A.

15
16 ⁶Current address: Department of Biochemistry, University of Missouri, Columbia, MO 65211.
17 U.S.A.

18
19 *Correspondence: jshorter@pennmedicine.upenn.edu

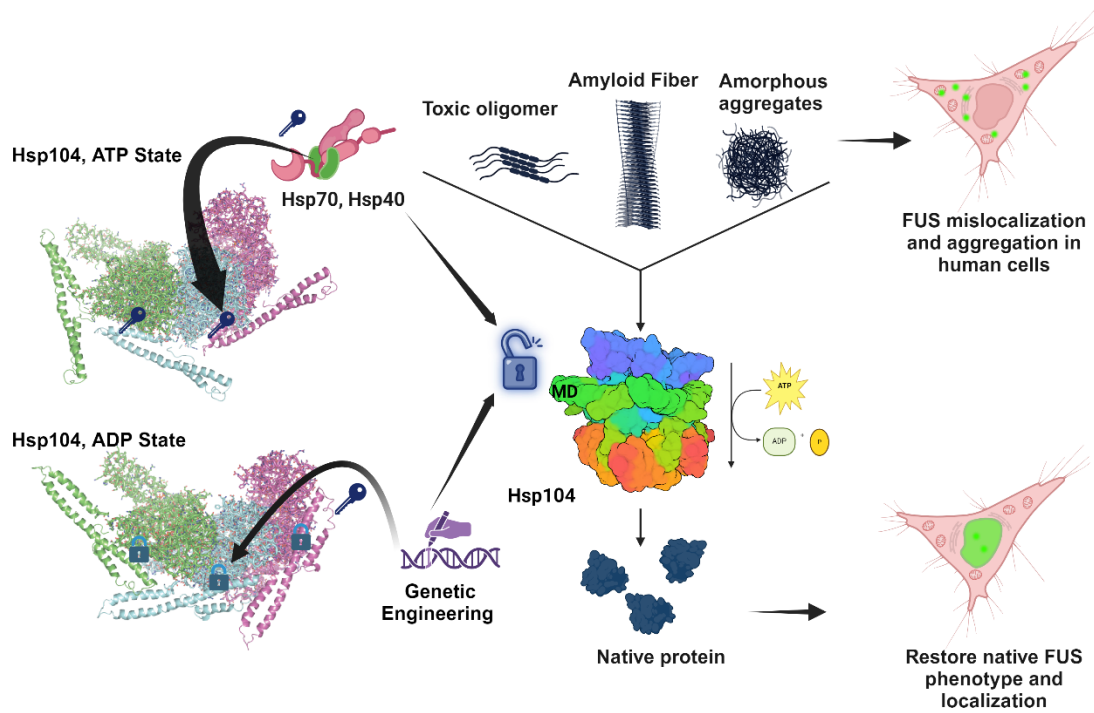
23 **Abstract**

24 The hexameric AAA+ disaggregase, Hsp104, collaborates with Hsp70 and Hsp40 via its
25 autoregulatory middle domain (MD) to solubilize aggregated protein conformers. However, how
26 ATP- or ADP-specific MD configurations regulate Hsp104 hexamers remains poorly understood.
27 Here, we define an ATP-specific network of interprotomer contacts between nucleotide-binding
28 domain 1 (NBD1) and MD helix L1, which tunes Hsp70 collaboration. Manipulating this network
29 can: (a) reduce Hsp70 collaboration without enhancing activity; (b) generate Hsp104 hypomorphs
30 that collaborate selectively with class B Hsp40s; (c) produce Hsp70-independent potentiated
31 variants; or (d) create species barriers between Hsp104 and Hsp70. Conversely, ADP-specific
32 intraprotomer contacts between MD helix L2 and NBD1 restrict activity, and their perturbation
33 frequently potentiates Hsp104. Importantly, adjusting the NBD1:MD helix L1 rheostat via rational
34 design enables finely tuned collaboration with Hsp70 to safely potentiate Hsp104, minimize off-
35 target toxicity, and counteract FUS proteinopathy in human cells. Thus, we establish important
36 design principles to tailor Hsp104 therapeutics.

37

38

39 Graphical Abstract



40

41

42 Introduction

43 Protein function requires high-fidelity protein folding.¹ However, in the cell, proteins are exposed
44 to various stresses such as translational errors, heat or chemical shock, and aging, which can
45 elicit protein misfolding and aggregation.² The accumulation of misfolded and aggregated proteins
46 is problematic and can be toxic.^{3,4} Thus, cells possess sophisticated molecular chaperones,
47 protein disaggregases, protein-degradation systems, and stress-response pathways to maintain
48 protein quality control.^{5,6} However, chronic accumulation of misfolded protein conformers upon
49 aging can yield aberrant protein fibrils that are intimately tied to fatal neurodegenerative
50 proteinopathies, such as α -synuclein fibrils in Parkinson's disease (PD), or TDP-43 and FUS fibrils
51 in amyotrophic lateral sclerosis (ALS).⁷⁻¹⁰ There are no effective treatments for these devastating
52 neurodegenerative disorders.

53
54 One strategy for these neurodegenerative diseases would be to develop therapeutic protein
55 disaggregases that liberate proteins trapped in aberrant oligomeric and aggregated states and
56 restore them to native solubility, form, and function.¹¹ Such agents would eliminate two malicious
57 problems associated with deleterious protein misfolding and aggregation: (1) the toxic gain of
58 function of aggregated conformers; and (2) the loss of protein function due to sequestration in
59 aggregated conformers.¹¹ Thus, we have focused on Hsp104, a ring-shaped, hexameric AAA+
60 (ATPase Associated with diverse Activities) protein disaggregase, which can suppress age-
61 related protein aggregation.¹¹⁻¹⁴ Notably, Hsp104 dissolves a diverse spectrum of aggregated
62 structures, including preamyloid oligomers, disordered aggregates, phase-separated
63 condensates, and stable amyloid or prion fibrils.¹⁵⁻²⁰ However, no exact Hsp104 homolog is found
64 in metazoa,^{11,21,22} although a related human mitochondrial AAA+ protein, Skd3, displays potent
65 disaggregase activity,²³⁻²⁶ and another AAA+ protein VCP/p97 may remodel ubiquitylated protein
66 inclusions in the cytoplasm.²⁷ Nonetheless, introduction of Hsp104 or engineered variants into
67 metazoan systems is well tolerated and can antagonize aggregation and toxicity of
68 neurodegenerative disease proteins.^{16,28-35}

69 Hsp104 is composed of two nucleotide-binding domains (NBD1 and NBD2) per monomer
70 separated by a middle domain (MD) and flanked by an N-terminal domain (NTD) and C-terminal
71 domain (CTD).¹³ The MD is an autoinhibitory domain that regulates Hsp104 disaggregase
72 activity.¹³ Indeed, single mutations in the MD can relieve autoinhibition and enhance Hsp104
73 disaggregase activity.³⁶⁻⁴¹ Precisely how the MD permits or restricts Hsp104 disaggregase activity
74 is not completely understood.

75 Hsp70 and Hsp40 enable optimal Hsp104 disaggregase activity.^{15,19,42-44} Hsp70s, and their
76 obligate cochaperones, Hsp40s, are highly conserved.⁴⁵ Hsp40 binds substrate proteins and
77 transfers them to Hsp70 via activation of Hsp70 ATPase activity.⁴⁶⁻⁴⁸ Interactions between Hsp70
78 and the NTD and MD of Hsp104 appear to enable disaggregase activity.^{13,49-51} However, the
79 precise mechanism by which Hsp104, Hsp70, and Hsp40 coordinate activity remains uncertain.
80 Several studies have utilized prokaryotic homologues of Hsp104 and Hsp70, ClpB and DnaK,
81 respectively.⁵²⁻⁵⁵ However, prokaryotic ClpB is unable to perform the complete repertoire of
82 eukaryotic Hsp104 activities.^{17,18,31,50,56,57} Indeed, there are several key structural and mechanistic
83 differences between Hsp104 and ClpB.^{50,57-61} Several interaction sites on the MD of ClpB are
84 proposed to interact with DnaK^{52,53} and the MD of Hsp104 has been proposed to interact with a
85 fragment of human Hsp70 (HSPA1A).⁴⁹ However, the structural determination of the Hsp104-
86 Hsp70 interaction has been difficult to resolve due to the weak and transient interactions between
87 these two proteins.^{52,53}

88 We have discovered many Hsp104 variants bearing single missense mutations in NBD1, MD, or
89 NBD2, which display enhanced disaggregase activity.^{29,30,36,58,62-65} However, some of these
90 Hsp104 variants, particularly MD or NBD1 variants, can present with "off-target" toxicity.^{29,30,63}
91 Specifically, overexpressing these Hsp104 variants in $\Delta hsp104$ yeast reduces growth at 37°C,
92 likely by unfolding metastable, soluble proteins.^{29,36} It has been suggested that Hsp70 might direct
93 Hsp104 to aggregated proteins rather than misfolded soluble substrates, which may prevent off-
94 target toxicity.⁶⁶ However, the mechanism of Hsp104-Hsp70 cooperation and its connection to
95 off-target toxicity is still poorly understood. Consequently, rational design of potentiated Hsp104
96 variants with no off-target toxicity remains a significant challenge.³⁰

97 Here, we address these challenges by exploring an intimate network of contacts between the MD
98 and NBD1 revealed in high-resolution cryogenic electron microscopy (cryo-EM) structures of
99 Hsp104.⁵⁹ We discover that the ATP-specific interactions between MD helix L1 and NBD1 of the
100 adjacent clockwise protomer are critical for collaboration between Hsp104 and Hsp70 in protein
101 disaggregation. Manipulating this network can: (a) reduce Hsp70 collaboration without enhancing
102 activity; (b) generate Hsp104 hypomorphs that collaborate selectively with class B Hsp40s; (c)
103 produce Hsp70-independent potentiated variants; or (d) create species barriers between Hsp104
104 and Hsp70. By contrast, the distinctive ADP-specific intraprotomer contacts between MD helix L2
105 and NBD1 restrict activity, and their perturbation frequently potentiates disaggregase activity. We
106 establish that the off-target toxicity of specific potentiated Hsp104 variants is determined by
107 reduced dependence on Hsp70 for protein disaggregation. By tuning the ATP-specific MD helix

108 L1 and NBD1 interaction, we can specify a desired level of Hsp70 collaboration to yield
109 potentiated Hsp104 variants with no off-target toxicity. Importantly, for the first time, we establish
110 that potentiated Hsp104 variants can mitigate FUS proteinopathy in human cells. Overall, our
111 findings establish important design principles to tailor therapeutic Hsp104 variants.

112

113 **Results**

114 **The MD changes orientation as Hsp104 hexamers switch from ATP-bound to ADP-bound** 115 **states, which alter NBD1:MD interactions**

116 The MD plays a critical role in regulating Hsp104 activity.^{13,29,67-69} High-resolution structures of
117 Hsp104 hexamers determined by cryo-EM reveal a dramatic change in the orientation of the MD
118 between the substrate-free AMP-PNP state (hereafter referred to as the ATP state) and substrate-
119 free ADP state (Figure 1A, B).^{59,70} Importantly, these two distinct states are also observed in
120 substrate-bound Hsp104 hexamers in the corresponding protomers bound to ATP or ADP,
121 indicating that these states are populated by distinct protomers during substrate translocation.⁵⁹
122 However, it has remained unclear precisely how Hsp104 activity is regulated by the distinct
123 interactions between NBD1 and the MD in either state.

124 We surveyed the interactions between NBD1 and the MD for each nucleotide state (Figure 1A,
125 B). Numerous contacts, including hydrophobic (red line), electrostatic (black line), and hydrogen
126 bond (blue line) interactions, are observed in both nucleotide states (Figure 1A, B, right). All the
127 interactions observed in protomer 3 (P3, in green) and protomer 4 (P4, in blue) are displayed for
128 the ATP state (Figure 1A, right) and ADP state (Figure 1B, right). Notably, in the ATP state we
129 find that helix L1 of the MD of protomer 4 makes several interprotomer contacts with NBD1 of the
130 adjacent clockwise protomer 3 (Figure 1A).⁷⁰

131 By contrast, in the ADP state, we find that interactions between NBD1 and the MD are completely
132 remodeled such that helix L2 of the MD now makes intraprotomer contacts with NBD1 (Figure
133 1B).⁵⁹ Moreover, in the ADP state, the precise NBD1:MD intraprotomer interactions are not
134 completely identical in different subunits. Some interactions are only present in P3 (shown in
135 green) or P4 (blue) (Figure 1B, right). Only a few interactions are the same in both protomers
136 (Figure 1B, shown in green and blue stripes), indicating diverse intraprotomer interactions
137 between the MD and NBD1 in this state. In addition to helix L2, helices L1 and L4 as well as the
138 loops between helix L2 and L3 and helix L4 and NBD1 also make intraprotomer contacts with
139 NBD1 (Figure 1B). Thus, the MD makes a radically different set of interactions with NBD1 in the
140 presence of ADP versus ATP.

141 We hypothesized that the interprotomer interactions between NBD1 and the MD in the ATP state
142 (Figure 1A) and intraprotomer interactions between NBD1 and the MD in the ADP state (Figure
143 1B) may play key roles in regulating Hsp104 activity. Thus, to investigate the mechanism by which
144 the MD regulates Hsp104 activity, we performed mutagenesis analysis to perturb the interactions

145 between NBD1 and the MD for each state. Remarkably, we find that perturbation of the
146 interprotomer NBD1-MD interactions of the ATP state has different functional consequences for
147 Hsp104 activity than perturbation of the intraprotomer NBD1-MD interaction of the ADP state.

148 **Interprotomer NBD1:MD interactions of the ATP state are essential for Hsp104** 149 **collaboration with Hsp70**

150 To alter interactions between NBD1 and MD helix L1 in the ATP state, we first modified the
151 charges of four of the NBD1:MD salt-bridge interactions: E190:R419, R194:E412, R353:E427,
152 and R366:D434 (Figure 1C). Thus, we constructed the opposite charge variants to perturb the
153 salt bridges: Hsp104^{E190K}, Hsp104^{R419E}, Hsp104^{R194E}, Hsp104^{E412K}, Hsp104^{R353E}, Hsp104^{E427K},
154 Hsp104^{R366E}, and Hsp104^{D434K}. Previously, we purified and measured the ATPase activity of
155 Hsp104^{R194E}, Hsp104^{E412K}, Hsp104^{R353E}, Hsp104^{E427K}, Hsp104^{R366E}, and Hsp104^{D434K}.⁵⁹ We found
156 that these Hsp104 variants display wild-type (WT) levels of ATPase activity, which is stimulated
157 by the disordered substrate casein.⁵⁹ However, these variants cannot work with human Hsp70
158 (Hsc70 [HSPA8]) and Hsp40 (DnaJA1) to disaggregate and reactivate firefly luciferase trapped in
159 chemically denatured aggregates.⁵⁹ We have now purified the remaining variants, Hsp104^{E190K}
160 and Hsp104^{R419E}, which possessed WT levels (Hsp104^{E190K}) or approaching WT levels (~70% for
161 Hsp104^{R419E}) of ATPase activity (Figure 1D). Hsp104^{E190K} and Hsp104^{R419E} also displayed limited
162 ability to work with human Hsc70 and DnaJA1 to disaggregate and reactivate luciferase (Figure
163 1E, pink bars). These findings suggest that perturbation of the MD helix L1 interactions with NBD1
164 of the adjacent clockwise protomer in the ATP state does not grossly affect ATPase activity but
165 reduces disaggregase activity.

166 It remained unclear, however, whether disruption of these contacts prevents Hsp104 from
167 coupling ATP hydrolysis to protein disaggregation or whether they specifically reduce
168 collaboration with Hsp70 and Hsp40. To distinguish between these possibilities, we first
169 established that these Hsp104 variants bind a model, disordered substrate, β -casein, with the
170 same affinity as Hsp104 (Figure S1A). Thus, substrate engagement appears unaffected by these
171 mutations. We next assessed the intrinsic disaggregase activity of the Hsp104 variants in the
172 presence of a 1:1 ratio of ATP and the slowly hydrolyzable ATP analog, ATP γ S. Hsp104
173 disaggregates and reactivates luciferase trapped in chemically denatured aggregates in the
174 presence of a 1:1 ratio of ATP:ATP γ S in the absence of Hsp70 and Hsp40,^{18,65,71} thereby allowing
175 assessment of whether the mutations perturbed the ability of Hsp104 to couple ATP hydrolysis to
176 protein disaggregation. We found that all the Hsp104 variants tested could disaggregate and
177 reactivate luciferase as well or better than WT Hsp104 under these conditions (Figure 1E, grey

178 bars). Indeed, Hsp104^{R194E} and Hsp104^{D434K} were more effective than Hsp104 (Figure 1E, grey
179 bars). However, unlike Hsp104, none of these Hsp104 variants could collaborate with human
180 Hsc70 and DnaJA1 to disaggregate and reactivate luciferase (Figure 1E, pink bars). These
181 findings suggest that perturbation of the MD helix L1 interactions with NBD1 of the adjacent
182 clockwise protomer in the ATP state can specifically impair Hsp70 collaboration and do not affect
183 the ability of Hsp104 to couple ATP hydrolysis to protein disaggregation.

184 We next tested the ability of these Hsp104 variants to confer induced thermotolerance (i.e., ability
185 to survive at 50°C after a 37°C pretreatment) in $\Delta hsp104$ yeast. Previously, we tested
186 Hsp104^{R194E}, Hsp104^{E412K}, Hsp104^{R353E}, Hsp104^{E427K}, Hsp104^{R366E}, or Hsp104^{D434K}, which were
187 unable to confer induced thermotolerance.⁵⁹ Hsp104^{R366E} displayed some limited activity, which
188 was greater than the other variants, but was still largely ineffective.⁵⁹ These findings suggest that
189 Hsp104 collaboration with Hsp70 and Hsp40 is critical for thermotolerance *in vivo*.⁷² We now
190 extend this analysis to Hsp104^{E190K} and Hsp104^{R419E}. Hsp104^{E190K} exhibited impaired activity as
191 with other NBD1:MD variants⁵⁹ (Figure 1F) and was expressed at similar levels to Hsp104 (Figure
192 1G). Surprisingly, however, Hsp104^{R419E} could confer induced thermotolerance like Hsp104 after
193 20min but displayed reduced activity at 30min (Figure 1F). Hsp104, Hsp104^{E190K}, and Hsp104^{R419E}
194 were all expressed at similar levels (Figure 1G). One possible explanation for the activity of
195 Hsp104^{R419E} and the residual activity of Hsp104^{R366E} might be an ability to collaborate with a
196 subset of Hsp70 or Hsp40 homologues in yeast.

197 **Residues and salt-bridge interactions in the interprotomer NBD1:MD helix L1 interface** 198 **regulate Hsp40 compatibility for Hsp104-Hsp70 disaggregase activity**

199 To assess this possibility, we purified yeast Hsp70 homologue, Ssa1, class A Hsp40, Ydj1, and
200 class B Hsp40, Sis1, to test their ability to collaborate with the Hsp104 variants in luciferase
201 disaggregation and reactivation *in vitro*. Hsp104^{E190K}, Hsp104^{R194E}, Hsp104^{E412K}, Hsp104^{R353E},
202 Hsp104^{E427K}, and Hsp104^{D434K} cannot disaggregate and refold luciferase in the presence of Ssa1
203 plus Sis1, Ssa1 plus Ydj1, or Ssa1 plus Sis1 and Ydj1 (Figure 2A). Thus, these Hsp104 variants
204 are severely impaired in collaboration with Ssa1, Sis1, and Ydj1. By contrast, Hsp104^{R419E} and
205 Hsp104^{R366E} displayed some activity in the presence of Ssa1 plus Sis1 or Ssa1 plus Sis1 and
206 Ydj1, but not Ssa1 plus Ydj1 (Figure 2A). Thus, Hsp104^{R419E} and Hsp104^{R366E} are selectively
207 defective in collaboration with the class A Hsp40, Ydj1.

208 We next asked whether Hsp104^{R419E} and Hsp104^{R366E} collaboration with Hsp70 was also
209 impaired. Thus, we tested the Ssa1 dose-dependent disaggregation activity of Hsp104 (positive

210 control), Hsp104^{R366E}, Hsp104^{R419E}, and Hsp104^{D434K} (negative control) in the absence of Hsp40.
211 Hsp104^{D434K} is incapable of working with Ssa1 to disaggregate luciferase, whereas Hsp104^{R419E}
212 and Hsp104^{R366E} remain partially active, but have reduced activity compared to Hsp104 (Figure
213 2B). Together with the yeast thermotolerance results (Figure 1F),⁵⁹ our findings suggest that
214 Hsp104^{E190K}, Hsp104^{R194E}, Hsp104^{E412K}, Hsp104^{R353E}, Hsp104^{E427K}, and Hsp104^{D434K} are
215 completely impaired for collaboration with Hsp70, whereas Hsp104^{R419E} and Hsp104^{R366E} can
216 partially work with Hsp70.

217 Next, we examined Hsp40 compatibility with Hsp104^{R419E} and Hsp104^{R366E} in more detail. Thus,
218 we assessed luciferase disaggregation and reactivation at fixed Hsp104^{R419E} or Hsp104^{R366E}
219 (1μM) and Ssa1 (0.167μM) concentrations with increasing amounts of Sis1 or Ydj1. Remarkably,
220 Hsp104^{R419E} and Hsp104^{R366E} were unable to collaborate with Ydj1 (Figure 2C), whereas they
221 could collaborate with Sis1 (Figure 2D). By contrast, Hsp104 and a canonical potentiated variant,
222 Hsp104^{A503S},²⁹ were active with Ydj1 or Sis1, although Ydj1 inhibited activity at high
223 concentrations, whereas Sis1 did not (Figure 2E, F). Notably, Hsp104^{A503S} is much more active
224 than Hsp104 at low Ydj1 concentrations (Figure S1B).²⁹ However, at the optimal Sis1 or Ydj1
225 concentrations, the disaggregase activities of Hsp104 and Hsp104^{A503S} are similar (Figure 2E, F).
226 Our findings suggest that Hsp104^{R419E} and Hsp104^{R366E} can partially work with Ssa1 (Figure 2B),
227 but their luciferase reactivation activity is more sensitive to inhibition by Ydj1 (Figure 2C). Thus,
228 Hsp104 collaboration with Ydj1 during luciferase disaggregation and reactivation requires R366
229 in NBD1 and R419 in MD helix L1.

230 **Ydj1 but not Sis1 can dissociate substrates from Hsp104 and inhibit the spontaneous** 231 **refolding of unfolded luciferase**

232 Bell-shaped reactivation curves were observed for all Hsp104 variants as a function of Ydj1
233 concentration, indicating that the synergistic cooperativity of Hsp104-Ssa1-Ydj1 is regulated by
234 the Ydj1 concentration (Figure 2C, E). In the tested concentration range, an inhibitory effect of
235 Sis1 on luciferase disaggregation and reactivation activity was not observed (Figure 2D, F). The
236 inhibition of protein disaggregation and reactivation by high Ydj1 concentrations could be due to
237 substrate competition between Ydj1 and Hsp104-Hsp70 complex, which may resemble the 'hook
238 effect' of proteolysis targeting chimera (PROTAC) molecules (i.e., high concentrations of a linker
239 [in this case Ydj1] suppresses formation of ternary complexes due to excessive formation of
240 binary complexes).⁷³ Additionally or alternatively, this effect might be explained by excess Ydj1
241 binding to unfolded luciferase released by Hsp104 and preventing it from refolding.

242 The class A Hsp40, Ydj1, has six sites involved with substrate binding in each dimer.⁷⁴ These
243 sites reside in client-binding domain 1 (CBD1), client-binding domain 2 (CBD2), and the zinc-
244 finger domain.⁷⁴ By contrast, the class B yeast Hsp40, Sis1, contains CBD1, but lacks CBD2.⁷⁴
245 Thus, Ydj1 may have a higher affinity for interacting with the substrate than Sis1, which might
246 compete with Hsp104 for substrate binding. To test this idea, we preformed Hsp104:β-casein
247 complexes in the presence of ATPγS and titrated in Ydj1 or Sis1. Hsp104^{R419E} and Hsp104^{R366E}
248 bind to casein with similar affinity as Hsp104 (Figure S1). As predicted, Ydj1 can compete for β-
249 casein (30nM) from Hsp104^{R419E}, Hsp104^{R366E}, and Hsp104 at an IC₅₀~20-40μM (Figure S2A,
250 Table S1), whereas Sis1 cannot (Figure S2B). This IC₅₀ value is similar to the IC₅₀ of Ydj1 for
251 inhibition of luciferase disaggregation and reactivation by Hsp104 at ~14μM (Figure 2C, Table
252 S1). By contrast, Hsp104^{R419E} and Hsp104^{R366E} are inhibited by much lower concentrations of Ydj1
253 in luciferase disaggregation and reactivation (Figure 2C and Table S1). These results suggest
254 that Ydj1 may compete for substrate binding to Hsp104, which may contribute to the inhibition of
255 Hsp104-mediated luciferase disaggregation and reactivation at high Ydj1 concentrations.
256 However, this mode of inhibition does not readily explain the inhibition of Hsp104^{R419E} and
257 Hsp104^{R366E} by low Ydj1 concentrations.

258 We wondered whether Ydj1 might inhibit the refolding of the small amounts of luciferase released
259 by Hsp104^{R419E} and Hsp104^{R366E}, which would severely restrict their luciferase reactivation
260 activity. Thus, we next tested whether Ydj1 or Sis1 can inhibit spontaneous refolding of soluble
261 unfolded luciferase. For this purpose, we unfold native luciferase (at the luciferase concentrations
262 indicated in Figure S2C) with 6M Urea on ice for 5min. We then dilute the soluble unfolded
263 luciferase into buffer and verified the spontaneous refolding of luciferase over 90 min (Figure
264 S2C). At high concentrations, Ydj1 can inhibit this spontaneous refolding of soluble luciferase, but
265 this inhibition is dependent on the luciferase concentration (Figure S2D). For low concentrations
266 of unfolded luciferase (1nM or 2nM), Ydj1 inhibits spontaneous refolding with an IC₅₀ of ~3μM
267 (Figure S2D). At higher concentrations of unfolded luciferase (10nM or 20nM), inhibition by Ydj1
268 is insignificant, and the IC₅₀ cannot be determined at the tested Ydj1 concentration range (Figure
269 S2D). By contrast, Sis1 does not inhibit luciferase refolding at all tested luciferase concentrations
270 (Figure S2E). These results indicate that when small amounts of luciferase are released from
271 aggregates by Hsp104, its refolding can be inhibited by excess Ydj1. We suggest that Hsp104
272 releases more unfolded luciferase than Hsp104^{R419E} and Hsp104^{R366E}, and thus higher Ydj1
273 concentrations are needed to inhibit Hsp104 than Hsp104^{R419E} or Hsp104^{R366E}. Collectively, these
274 findings suggest that reduced ability to collaborate with Ssa1 and inhibition by Ydj1 render
275 Hsp104^{R419E} and Hsp104^{R366E} hypomorphic *in vitro* and *in vivo*. These findings also emphasize

276 the importance of Hsp104 collaboration with Ssa1 and Ydj1 for thermotolerance *in vivo*, as the
277 Hsp104 variants that can only work with Ssa1 and Sis1 are hypomorphic.^{72,75,76}

278 **Rewiring the interprotomer NBD1:MD helix L1 interaction alters Hsp104 collaboration with** 279 **Hsp70 and Hsp40**

280 We next tested whether rewiring salt-bridge interactions between NBD1 and MD helix L1 could
281 restore Hsp104 collaboration with Hsp70 and Hsp40. Thus, we generated Hsp104^{E190K:R419E},
282 Hsp104^{E190R:R419E}, Hsp104^{R194E:E412K}, Hsp104^{R353E:E427K}, Hsp104^{R353E:E427R}, Hsp104^{R366E:D434K}, and
283 Hsp104^{R366E:D434R}, which would be predicted to have reconstructed salt bridges between NBD1
284 and MD helix L1 in the ATP state (Figure 1C). However, in these variants the location of the acidic
285 and basic partner residues is reversed compared to Hsp104.

286 We first assessed the activity of these Hsp104 variants in luciferase disaggregation and
287 reactivation. To our surprise, Hsp104^{E190K:R419E} and Hsp104^{E190R:R419E} show enhanced activity
288 compared to Hsp104 in the absence or presence of human Hsc70 and DnaJA1 (Figure 3A).
289 Remarkably, Hsp104^{E190R:R419E} exhibited similar activity with or without Hsc70 and DnaJA1 (Figure
290 3A). The increased level of activity of Hsp104^{E190K:R419E} and Hsp104^{E190R:R419E} and their
291 independence from Hsp70 is consistent with potentiated Hsp104 activity.^{29,30,40,51,58,63,64} Indeed,
292 these variants also exhibited increased ATPase activity, another indicator of potentiated activity
293 (Figure S3A).^{29,30,40,51,58,63,64} Thus, altering the charge orientation of the salt bridge between
294 position 190 of NBD1 and position 419 of MD helix L1 potentiates Hsp104 activity (Figure 3A).
295 Intriguingly, this potentiated activity was only uncovered at this position of the NBD1:MD helix L1
296 interaction, which may pinpoint a precise location where Hsp70 activates Hsp104.

297 Indeed, Hsp104^{R194E:E412K}, Hsp104^{R353E:E427K}, Hsp104^{R353E:E427R}, Hsp104^{R366E:D434K}, and
298 Hsp104^{R366E:D434R} were inactive for luciferase disaggregation and reactivation in the presence or
299 absence of human Hsc70 and DnaJA1 (Figure 3A). These variants retained ATPase activity, but
300 it was reduced in comparison to Hsp104 (Figure S3A). To determine activity *in vivo*, we assessed
301 their ability to confer induced thermotolerance in $\Delta hsp104$ yeast. As expected, Hsp104^{R194E:E412K},
302 Hsp104^{R194E:E412R}, Hsp104^{R353E:E427K}, and Hsp104^{R366E:D434K} were unable to confer induced
303 thermotolerance (Figure 3B). To our surprise, however, Hsp104^{R353E:E427R} and Hsp104^{R366E:D434R}
304 conferred induced thermotolerance to ~67% of the level conferred by Hsp104 (Figure 3B). These
305 Hsp104 variants were expressed at similar levels (Figure S3B). Thus, Hsp104^{R353E:E427R} and
306 Hsp104^{R366E:D434R} are functional *in vivo* but fail to collaborate with human Hsc70 and DnaJA1 *in*
307 *vitro* (Figure 3A, B).

308 To understand the concordance (for Hsp104^{R194E:E412K}, Hsp104^{R353E:E427K}, and Hsp104^{R366E:D434K})
309 and discordance (for Hsp104^{R353E:E427R} and Hsp104^{R366E:D434R}) between the *in vitro* and *in vivo*
310 data, we further dissected the activity of these variants *in vitro*. First, we found that the intrinsic
311 luciferase disaggregation and reactivation activity of Hsp104^{R194E:E412K}, Hsp104^{R353E:E427K} and
312 Hsp104^{R366E:D434K} in the presence of ATP:ATPγS and the absence of Hsp70 and Hsp40 was like
313 Hsp104 (Figure 3C). Thus, these variants can couple ATP hydrolysis to protein disaggregation
314 and reactivation, indicating a specific defect in collaboration with Hsp70 and Hsp40. These data
315 reinforce the concept that the ATP-specific NBD1:MD helix L1 interaction is critical for
316 collaboration with Hsp70 and Hsp40.

317 Next, we assessed whether the functional interaction with Ssa1 was affected. Thus, we assessed
318 luciferase disaggregation and reactivation in the presence of ATP plus Ssa1, but in the absence
319 of Hsp40. Here, none of the variants had levels of activity comparable to Hsp104 (Figure 3D).
320 Indeed, Hsp104^{R194E:E412K} and Hsp104^{R366E:D434K} were inactive, whereas Hsp104^{R353E:E427K} and
321 Hsp104^{R366E:D434R} exhibited limited activity (Figure 3D). Hsp104^{R353E:E427R} exhibited ~40% Hsp104
322 activity, which is consistent with the ability of this variant to confer some induced thermotolerance
323 (Figure 3B). Nonetheless, these findings suggest that these Hsp104 variants have reduced ability
324 to collaborate directly with Ssa1.

325 We then added the class B Hsp40, Sis1, or class A Hsp40, Ydj1, together with Ssa1 and assessed
326 luciferase disaggregation and reactivation activity (Figure 3E, F). Here, Hsp104^{R194E:E412K} and
327 Hsp104^{R366E:D434K} are inactive with Ssa1 plus Sis1 or Ydj1 (Figure 3E, F), which explains the
328 inability of these Hsp104 variants to confer induced thermotolerance (Figure 3B).
329 Hsp104^{R353E:E427K} and Hsp104^{R366E:D434R} both exhibited ~60% of Hsp104 activity with Ssa1 plus
330 Sis1 (Figure 3E), and limited activity with Ssa1 and Ydj1 (Figure 3F). Hsp104^{R366E:D434R} (~24% of
331 Hsp104) was slightly more active with Ssa1 and Ydj1 than Hsp104^{R353E:E427K} (~15% of Hsp104)
332 (Figure 3F), which may help explain why Hsp104^{R366E:D434R} confers some induced thermotolerance
333 in yeast, whereas Hsp104^{R353E:E427K} confers limited induced thermotolerance (Figure 3B).

334 Notably, Hsp104^{R353E:E427R} displayed WT levels of activity with Ssa1 and Sis1 (Figure 3E) and
335 ~42% Hsp104 activity with Ssa1 and Ydj1 (Figure 3F), which helps explain why this variant
336 confers induced thermotolerance *in vivo* (Figure 3B), despite limited activity with human Hsc70
337 and DnaJA1 (Figure 3A). Indeed, it appears that the reconfigured NBD1:MD helix L1 salt bridge
338 of Hsp104^{R353E:E427K}, Hsp104^{R353E:E427R}, and Hsp104^{R366E:D434R} creates a species barrier between
339 yeast Hsp104 and human Hsc70 and DnaJA1, i.e., Hsp104^{R353E:E427K}, Hsp104^{R353E:E427R}, and
340 Hsp104^{R366E:D434R} do not work well with human Hsc70 and DnaJA1 but are functional with yeast

341 Ssa1 and Ydj1. Thus, it appears that the interprotomer interactions between NBD1 and MD helix
342 L1 of the ATP state can be altered to establish species barriers between Hsp104 and Hsp70,
343 which can occur naturally as with the barrier between yeast Hsp104 and bacterial Hsp70.^{15,67}

344 Collectively, these results reveal the ATP-specific interprotomer interactions between NBD1 and
345 MD helix L1 (Figure 1A) function as a rheostat to fine-tune Hsp104 collaboration with Hsp70 and
346 Hsp40. Perturbation of these contacts can reduce Hsp70 and Hsp40 collaboration without
347 potentiating activity (Figure 2A). Surprisingly, specific perturbation of this network yields
348 hypomorphic Hsp104 variants that collaborate selectively with class B Hsp40s as with
349 Hsp104^{R419E} and Hsp104^{R366E} (Figure 2A, C, D). Additionally, specific rewiring of this network
350 potentiates Hsp104 activity as with Hsp104^{E190K:R419E} and Hsp104^{E190R:R419E} (Figure 3A). Rewiring
351 the network in other ways can greatly reduce collaboration with Hsp70 and Hsp40 without
352 affecting the intrinsic disaggregase activity of Hsp104 as with Hsp104^{R194E:E412K} and
353 Hsp104^{R366E:D434K} (Figure 3C-F). Remarkably, reconfiguring the NBD1:MD helix L1 network in yet
354 further ways can create species barriers with human Hsp70 as with Hsp104^{R353E:E427R} and
355 Hsp104^{R366E:D434R} (Figure 3A, E, F). Hsp104^{R353E:E427R} and Hsp104^{R366E:D434R} operate more similarly
356 to Hsp104 with the class B Hsp40, Sis1, but exhibit reduced activity with class A Hsp40, Ydj1
357 (Figure 3E, F), and confer up to ~67% of WT Hsp104 levels of induced thermotolerance *in vivo*
358 (Figure 3B). This finding suggests that collaboration with just Sis1 is insufficient for Hsp104 to
359 confer induced thermotolerance *in vivo*. Indeed, collaboration with Sis1 and Ydj1 appears critical
360 for WT levels of Hsp104 activity *in vivo*.⁷⁷ Overall, we conclude that ATP-specific interprotomer
361 interactions between NBD1 and MD helix L1 control several aspects of collaboration between
362 Hsp104 and Hsp70 plus Hsp40.

363 **Perturbing the intraprotomer NBD1:MD contacts of the ADP state frequently potentiates** 364 **Hsp104 activity**

365 In contrast to the ATP state, the MD primarily interacts with NBD1 within the same subunit of the
366 hexamer in the presence of ADP (Figure 1B). The role of these intraprotomer contacts in
367 comparison to the interprotomer NBD1:MD contacts of the ATP state has remained unclear.
368 Therefore, we explored 31 interactions involving 14 NBD1 residues and 19 MD residues in the
369 interaction surface presented in Figure 1B. We designed 46 mutations aiming to alter these
370 interactions, of which 16 have been tested previously.^{29,30,39,58,59,63} Thus, we generated 30
371 additional single missense Hsp104 variants expected to alter the interactions of this interface
372 (Table S2 and Figure 1B).

373 We then assessed these Hsp104 variants for the ability to suppress the toxicity of α -synuclein,
374 FUS, and TDP-43 in $\Delta hsp104$ yeast.²⁹ Here, Hsp104 and the vector control are unable to mitigate
375 α -synuclein, FUS, and TDP-43 toxicity, whereas positive control potentiated Hsp104 variants,
376 Hsp104^{A503V} or Hsp104^{A503S}, strongly suppress toxicity.²⁹ We find that ~72% (33/46) of the Hsp104
377 variants designed to weaken the intraprotomer NBD1-MD interactions of the ADP state potentiate
378 activity and enable mitigation of α -synuclein, FUS, and TDP-43 toxicity (Table S2). Among the 30
379 Hsp104 variants tested in this work, we found an additional 18 variants that enhanced activity and
380 an additional 12 variants that did not (Figure 4 and Table S2). Among the 18 potentiated variants,
381 only two variants (I361K and K470D) present off-target toxicity to yeast at 37°C (Figure S4A).
382 Moreover, the expression level of Hsp104 variants in yeast is verified (Figure S4B) and all 30
383 Hsp104 variants are expressed. These results suggest that the intraprotomer NBD1-MD-
384 interactions observed in the ADP state function to restrict Hsp104 activity. However, Hsp104
385 disaggregation activity can be unleashed by weakening these intraprotomer NBD1-MD-
386 interactions, resulting in potentiated variants with low off-target toxicity.

387 Among the 18 potentiated variants discovered in this work, Hsp104^{Y466C}, Hsp104^{K480C},
388 Hsp104^{K481E}, Hsp104^{R496D}, Hsp104^{I537A}, and Hsp104^{I537R} present strong activity in mitigating α -
389 synuclein, FUS, and TDP-43 toxicity with minimal off-target toxicity, and resemble Hsp104^{A503S}
390 (Figure 4 and S4A).²⁹ By contrast, Hsp104^{I361K}, Hsp104^{Y466K}, Hsp104^{K470D}, Hsp104^{H473S},
391 Hsp104^{K480L}, Hsp104^{K481L} and Hsp104^{E521R} show slightly reduced activity compared to
392 Hsp104^{A503S} (Figure 4), whereas Hsp104^{R179D}, Hsp104^{R407E}, Hsp104^{D408K}, and Hsp104^{D408V} were
393 further reduced, but still can mitigate α -synuclein, FUS, and TDP-43 toxicity (Figure 4).
394 Hsp104^{L414K} presents the lowest activity of the 18 new potentiated Hsp104 variants (Figure 4).
395 Hsp104^{L414K} mitigates α -synuclein and FUS toxicity but is unable to reduce TDP-43 toxicity (Figure
396 4). Interestingly, a valine scan of the entire MD only identified Hsp104^{R496V} and Hsp104^{K480V} with
397 potentiated activity among these same sites,³⁹ highlighting the power of making rational, targeted
398 mutations to potentiate activity.

399 **Restricting Hsp104 activity in the absence of Hsp70 reduces off-target toxicity of** 400 **potentiated Hsp104 variants**

401 Potentiated Hsp104 variants can exhibit unfavorable off-target toxicity, especially at 37°C in
402 yeast.^{29,30,63} Hsp104 likely recognizes unfolded regions of proteins with a bias for peptides of a
403 certain amino-acid composition rather than any specific sequence.⁷⁸ Thus, it was proposed that
404 potentiated Hsp104 variants may recognize and unfold metastable proteins, which results in
405 toxicity.^{29,63} One concept is that Hsp70 may direct Hsp104 to aggregated structures and away

406 from soluble misfolded polypeptides or naturally metastable proteins.⁶⁶ Since potentiated Hsp104
407 variants can function independently of Hsp70 to varying extents,^{29,30,63,64} this mechanism of
408 substrate selection may become dysregulated such that excessive soluble polypeptide unfolding
409 drives off-target toxicity. However, WT Hsp104 is too tightly regulated and is unable to overcome
410 widespread aggregation by neurodegenerative disease proteins such as TDP-43, FUS, and α -
411 synuclein in yeast.^{29,30,63,64} Thus, we hypothesize that potentiated Hsp104 variants with reduced
412 unfoldase activity for soluble proteins, and partial independence from Hsp70 may reside in an
413 advantageous therapeutic window. These Hsp104 variants would preferentially target aggregated
414 proteins without excessive and toxic unfolding of soluble proteins. Thus, we set out to test whether
415 potentiated Hsp104 variants with greater off-target toxicity have stronger unfoldase activity
416 against soluble proteins and less dependence on Hsp70 for protein disaggregation.

417 To test this concept, we selected several Hsp104 variants with a range of off-target toxicities:
418 Hsp104 (no off-target toxicity), Hsp104^{S535E} (an MD variant with minimal off-target toxicity),
419 Hsp104^{E360R} (an NBD1 variant with minimal off-target toxicity), and Hsp104^{I187F} (an NBD1 variant
420 with significant off-target toxicity) (Figure 5A).^{29,63,64} We then assessed the ability of these Hsp104
421 variants to unfold the model substrate RepA₁₋₁₅-GFP, which is comprised of the N-terminal 15
422 residues of RepA appended to the N-terminus of GFP.⁷⁹ The RepA₁₋₁₅ tag is a short, unfolded
423 region, which is sufficient to target RepA₁₋₁₅-GFP for unfolding by potentiated Hsp104 variants.
424 By contrast, Hsp104 does not unfold RepA₁₋₁₅-GFP in the presence of ATP (Figure 5B). Strikingly,
425 however, we find Hsp104^{I187F}, which has the most off-target toxicity, unfolds RepA₁₋₁₅-GFP the
426 most rapidly, whereas the less toxic Hsp104 variants, Hsp104^{S535E} and Hsp104^{E360R} unfold RepA₁₋₁₅-
427 GFP less rapidly than Hsp104^{I187F} (Figure 5B). Hence, off-target toxicity correlates positively
428 with stronger unfoldase activity against soluble protein.

429 To measure the Hsp70 dependence for Hsp104 disaggregase activity, we performed luciferase
430 disaggregation and reactivation experiments in the absence of Hsp70 or Hsp40 (Figure 5C). Here,
431 we find that Hsp104^{I187F} has the highest luciferase disaggregation and reactivation activity in the
432 absence of Hsp70 or Hsp40 (Figure 5C). By contrast, Hsp104^{E360R} and Hsp104^{S535E} show
433 significantly lower activity in the absence of Hsp70 and Hsp40, whereas Hsp104 is completely
434 inactive as expected (Figure 5C).¹⁵ Thus, off-target toxicity correlates positively with stronger
435 disaggregase activity in the absence of Hsp70 or Hsp40.

436 Next, we titrated Ssa1 (in the absence of Hsp40) into luciferase disaggregation and reactivation
437 experiments with each potentiated Hsp104 variant versus Hsp104. Hsp104^{I187F} shows very little
438 dependence on Ssa1 compared to Hsp104 (Figure 5D). By contrast, Hsp104^{E360R} shows stronger

439 dependence on Ssa1, but outperforms Hsp104 at every Hsp70 concentration tested (Figure 5E).
440 Intriguingly, Hsp104^{S535E} also shows Ssa1 dependence, but is greatly stimulated at high Ssa1
441 concentrations (Figure 5F). Thus, potentiated Hsp104 variants with minimal off-target toxicity are
442 also more dependent on Hsp70 in protein disaggregation.

443 **Rationally designed potentiated Hsp104 with minimized off-target toxicity**

444 Next, we developed Hsp104 variants with minimized off-target toxicity based on the design
445 principles established above, i.e., reduced unfoldase activity for soluble proteins and partial
446 independence from Hsp70 for protein disaggregation. Given that the ATP-specific interprotomer
447 NBD1:MD helix L1 interface functions as a rheostat for collaboration with Hsp70 and Hsp40
448 (Figure 2, 3), we focused on this region to define modifications that tune Hsp70-Hsp40
449 collaboration to the desired level.

450 Upon closer inspection of this salt bridge interaction, we observed that E190, E191, and E192 of
451 NBD1 are positioned such that they could all potentially contact R419 (Figure 6A, left panel).
452 E190, E191, and E192 are located at a loop between Helix B2 and B3 in NBD1 that forms a
453 junction with the coiled-coil MD helix L1 (Figure 6A, left panel). This loop may provide enough
454 freedom for these residues to have a dynamic interaction with R419. To test if salt-bridge
455 interactions between E190, E191, or E192 and R419 can regulate Hsp104 activity and
456 collaboration with Hsp70 and Hsp40, we designed variants to rewire these interactions and modify
457 MD orientation. Thus, we explored combinations of R419E with arginine substitutions at E190,
458 E191, or E192. We tested whether these designed variants could mitigate α -synuclein, FUS, and
459 TDP-43 toxicity in yeast and whether they exhibited off-target toxicity. All the Hsp104 variants
460 were expressed at roughly similar levels and did not affect disease protein expression (Figure
461 S5).

462 Previously, we found that Hsp104^{E190K:R419E} and Hsp104^{E190R:R419E} have enhanced disaggregase
463 activity (Figure 3A). However, this activity was largely independent of Hsp70 and Hsp40, which
464 predicts off-target toxicity (Figure 3A). In yeast, we found that these Hsp104 variants weakly
465 suppressed α -synuclein toxicity (Figure 6B) but were unable to suppress FUS toxicity (Figure 6C),
466 and very weakly suppressed TDP-43 toxicity (Figure 6D). This pattern of disease protein toxicity
467 mitigation is unusual and has not been observed before.^{29,30,37,58,63,64} Moreover, as predicted,
468 these variants exhibited off-target toxicity at 37°C (Figure 6E). Hence, the E190K/R:R419E
469 variants have the rheostat dialed too far toward Hsp70 independence (Figure 6A, right panel).

470 By contrast, Hsp104^{E191R:R419E} and Hsp104^{E192R:R419E} strongly suppress α -synuclein, FUS, and
471 TDP-43 toxicity (Figure 6B-D). Importantly, these variants did not exhibit off-target toxicity (Figure
472 6E). Hence, the E191R:R419E and E192R:R419E variants have the rheostat dialed to an
473 appropriate level of Hsp70 collaboration (Figure 6A, right panel).

474 Based upon these observations, we would predict that Hsp104^{E190R:R419E} would unfold RepA₁₋₁₅-
475 GFP more rapidly than Hsp104^{E191R:R419E} and Hsp104^{E192R:R419E}. We would also predict that
476 Hsp104^{E190R:R419E} would be less dependent on Hsp70 than Hsp104^{E191R:R419E} and Hsp104^{E192R:R419E}
477 for luciferase disaggregation and reactivation. These predictions were confirmed experimentally
478 (Figure 6F, G). Collectively, these findings suggest that interactions between NBD1 residues
479 E190, E191, or E192 and MD helix L1 R419 function as a rheostat that can be adjusted to fine-
480 tune collaboration with Hsp70.

481 **Potentiated Hsp104 variants suppress FUS proteinopathy in human cells**

482 A feature of degenerating neurons in various FUS proteinopathies, including ALS and
483 frontotemporal dementia (FTD), is the depletion of FUS from the nucleus and the accumulation
484 of FUS in cytoplasmic inclusions.¹⁰ Potentiated Hsp104 variants can mitigate cytoplasmic FUS
485 aggregation and toxicity in yeast,²⁹ but their activity in human cells has not been assessed. To
486 this end, we utilized a human (HeLa) cell model by expressing mCherry-tagged Hsp104 and GFP-
487 tagged FUS in HeLa cells.⁸⁰ We selected a panel of potentiated variants with minimal off-target
488 toxicity to assess in this system. Importantly, potentiated Hsp104 variants can significantly
489 suppress FUS cytoplasmic mislocalization and aggregation, whereas Hsp104 cannot (Figure 7A).
490 Indeed, Hsp104^{A503S}, Hsp104^{E191R:R419E}, Hsp104^{E360R}, Hsp104^{K481E}, and Hsp104^{S535E} suppressed
491 cytoplasmic FUS aggregation and maintained FUS in the nucleus (Figure 7A, B) without reducing
492 FUS expression level (Figure 7C). Thus, enhanced Hsp104 variants provide a mechanism to
493 mitigate aberrant cytoplasmic FUS aggregation in human cells.

494

495

496 Discussion

497 In this work, we performed an intensive structure-function analysis of how ATP-specific or ADP-
498 specific MD configurations regulate Hsp104 disaggregase activity. We determined that the ATP-
499 specific interactions between MD helix L1 and NBD1 of the adjacent clockwise protomer are
500 critical for Hsp104 to collaborate effectively with Hsp70 and Hsp40 during protein disaggregation.
501 Specifically, salt-bridge interactions between NBD1:MD L1 via E190:R419, R194:E412,
502 R353:E427, and R366:D434, enable Hsp104 to collaborate with Hsp70 and Hsp40. Intriguingly,
503 disrupting these interactions does not potentiate activity or affect the intrinsic disaggregase
504 activity of Hsp104. Thus, Hsp104 can still couple ATP hydrolysis to substrate processing when
505 these contacts are broken. However, the ability of Hsp104 to collaborate with Hsp70 and Hsp40
506 is specifically disrupted. These findings are surprising as it was anticipated that these interactions
507 would be important for intersubunit collaboration within the hexamer rather than collaboration with
508 Hsp70 and Hsp40.

509 Intriguingly, we find that specific perturbations of the ATP-specific NBD1:MD helix L1 interactions
510 (i.e., R419E or R366E) yielded hypomorphic Hsp104 variants. These Hsp104 hypomorphs confer
511 some thermotolerance *in vivo*. In luciferase disaggregation and reactivation *in vitro*, Hsp104^{R419E}
512 and Hsp104^{R366E} work selectively with Ssa1 and Sis1, and are unable to function with Ssa1 and
513 Ydj1 or human Hsc70 and DnaJA1. Thus, these Hsp104 variants displayed selectivity to function
514 with the class B Hsp40, Sis1, but not class A Hsp40s, Ydj1 or DnaJA1. Hsp104^{R419E} and
515 Hsp104^{R366E} were also less able to directly collaborate with Ssa1 directly (i.e., in the absence of
516 Hsp40) and were inhibited by Ydj1. These findings emphasize the importance of ATP-specific
517 NBD1:MD helix L1 interactions for productive collaboration with Hsp70 and class A Hsp40s.
518 Moreover, they reinforce the importance of Hsp104 collaboration with Ssa1 and Ydj1 for
519 thermotolerance *in vivo*.^{72,75,76}

520 Having identified the critical importance of ATP-specific NBD1:MD helix L1 interprotomer
521 interactions, we next assessed the consequences of rewiring these connections. Notably,
522 rebuilding the E190:R419 salt bridge to E190R:R419E or E190K:R419E yielded potentiated
523 Hsp104 variants, which functioned independently of Hsp70. Remarkably, reconfiguring the
524 NBD:MD helix L1 network in yet further ways can create species barriers with human Hsp70 as
525 with Hsp104^{R353E:E427R} and Hsp104^{R366E:D434R}. Thus, manipulating the network of ATP-specific
526 NBD1:MD helix L1 interprotomer interactions can: (a) reduce Hsp70 collaboration without
527 enhancing activity; (b) generate hypomorphic Hsp104 variants that collaborate selectively with
528 class B Hsp40s; (c) produce Hsp70-independent potentiated variants; or (d) create species

529 barriers between Hsp104 and Hsp70. Collectively, these findings suggest that the ATP-specific
530 NBD1: MD helix L1 interactions function as a rheostat to tune the level of collaboration with Hsp70
531 and Hsp40. Indeed, the ATP-specific network of interprotomer contacts between NBD1 and MD
532 helix L1 appears to be poised as a capacitor that can release diverse phenotypes.

533 By contrast, the ADP-specific intraprotomer contacts between NBD1 and MD helix L2 function to
534 restrict activity. When these contacts were disrupted (Figure 4 and Table S2), we observed
535 enhanced Hsp104 activity in mitigating α -syn, FUS and TDP-43 toxicity in yeast, indicating
536 enhanced disaggregase activity of these variants. Indeed, we designed 46 variants to alter 31
537 ADP-specific intraprotomer contacts, and 33 variants exhibited potentiated activity (Figure 4 and
538 Table S2). Disrupting these contacts likely increases the rate of ADP release from NBD1, which
539 accelerates the Hsp104 motor.⁴⁰ Notably, many residues, such as D233, E360, E366, E412, and
540 R419, are involved in both intraprotomer and interprotomer contacts between NBD1 and the MD,
541 indicating a dynamic and highly regulated network of interactions, which likely enable
542 communication within and between subunits during disaggregation.

543 A difficulty in developing potentiated Hsp104 variants as therapeutic agents lies in their off-target
544 toxicity, which likely stems from their ability to unfold, metastable soluble proteins or soluble
545 proteins with partially unfolded regions.³⁶ One solution to this problem is to increase the substrate
546 specificity of potentiated Hsp104 variants for specific neurodegenerative-disease proteins, which
547 we have achieved with α -synuclein.³⁰ However, multiple proteins can aggregate in
548 neurodegenerative disease, which may limit the utility of substrate-specific protein disaggregases.
549 Another strategy would be to tune Hsp104 activity such that potentiated disaggregase activity is
550 retained while unfolding of soluble proteins is minimized. Here, we establish that fine-tuning the
551 level of Hsp70 collaboration provides a mechanism to achieve this goal. We reach this conclusion
552 by first considering three potentiated Hsp104 variants: Hsp104^{I187F}, Hsp104^{E360R}, and
553 Hsp104^{S535E}.^{63,64} Hsp104^{I187F} exhibits more off-target toxicity than Hsp104^{E360R}, which in turn
554 exhibits more off-target toxicity than Hsp104^{S535E}.^{63,64} Strikingly, Hsp104^{I187F} unfolds RepA₁₋₁₅-
555 GFP (a model soluble protein with a partially unfolded region) more rapidly than Hsp104^{E360R},
556 which in turn unfolds RepA₁₋₁₅-GFP more rapidly than Hsp104^{S535E}. Furthermore, Hsp104^{I187F}
557 displays less dependence on Hsp70 than Hsp104^{E360R} or Hsp104^{S535E} in luciferase disaggregation
558 and reactivation. Thus, too much independence from Hsp70 may yield off-target toxicity, whereas
559 too much dependence of Hsp70 (as with wild-type Hsp104) leads to a reduced ability to combat
560 deleterious protein misfolding connected with neurodegenerative disease. Overall, our findings
561 suggest rules for minimizing off-target toxicity: (1) minimize the ability of the Hsp104 variant to

562 unfold soluble proteins with partially unfolded regions; and (2) tune the level of collaboration with
563 Hsp70.

564 We then leveraged this knowledge to adjust the ATP-specific NBD1:MD helix L1 rheostat to the
565 appropriate level of Hsp70 collaboration. We find that Hsp104^{E190R:R419E} displays increased off-
566 target toxicity, enhanced ability to unfold RepA₁₋₁₅-GFP, and less dependence on Hsp70 in
567 luciferase disaggregation and reactivation. By contrast, Hsp104^{E191R:R419E} and Hsp104^{E192R:R419E}
568 display reduced off-target toxicity, reduced ability to unfold RepA₁₋₁₅-GFP, and more dependence
569 on Hsp70 in luciferase disaggregation and reactivation. Hence, these NBD1:MD helix L1 variants
570 may set the ATP-specific MD configuration in a way that optimally tunes Hsp70 collaboration to
571 yield potentiated Hsp104 variants with minimal off-target toxicity.

572 Finally, we establish that potentiated Hsp104 variants with minimal off-target effects can mitigate
573 aberrant FUS aggregation in human cells for the first time. Thus, a panel of potentiated Hsp104
574 variants can reduce cytoplasmic FUS aggregation in human cells, whereas Hsp104 is ineffective.
575 These findings suggest that Hsp104 and enhanced variants can be translated to reduce
576 deleterious protein aggregation in human cells, which sets the stage for further developing
577 Hsp104 as a therapeutic agent. Indeed, in this light, advances in lipid nanoparticle-mediated
578 mRNA therapeutics are particularly exciting as they provide a mechanism to introduce a transient
579 dose of Hsp104 variants to where they are needed.^{81,82} In this way, potentiated Hsp104 variants
580 could relieve toxic protein aggregation and then be downregulated such that potential off-target
581 effects are minimized.

582 **STAR Methods**

583 **Key resources table**

REAGENT or RESOURCE	SOURCE	IDENTIFIER
Antibodies		
Rabbit anti-Hsp104 polyclonal	Enzo Life Sciences	Cat# ADI-SPA-1040-F; RRID: AB_2039208
Rabbit anti-FUS polyclonal	Bethyl Laboratories	Cat# A300-302A; RRID: AB_309445
Rabbit anti-TDP-43 polyclonal	Proteintech	Cat# 10782; RRID: AB_615042
Rabbit anti-GFP polyclonal	Sigma-Aldrich	Cat# G1544; RRID: AB_439690
Rabbit monoclonal anti-alpha tubulin antibody	Abcam	Cat# ab6160
Mouse anti-PGK1 monoclonal	Thermo Fisher	Cat# 459250; RRID: AB_2532235
Anti-mCherry polyclonal antibody	Abcam	Cat# ab167453
IRDye 800CW Goat anti-Mouse IgG secondary antibody	LI-COR	Cat# 926-32210; RRID:AB_621842
IRDye 680RD Goat anti-Rabbit IgG secondary antibody	LI-COR	Cat# 926-68071; RRID: AB_10956166
IRDye 800CW Goat anti-Rat IgG Secondary Antibody	LI-COR	Cat#926-32219; RRID: AB_1850025
Bacterial and virus strains		
<i>Escherichia coli</i> DH5 α competent cells	Thermo Fisher	Cat# 18265017
<i>Escherichia coli</i> BL21-CodonPlus (DE3) -RIL competent cells	Agilent	Cat# 230245
One Shot TOP10 Chemically Competent <i>Escherichia coli</i>	Invitrogen	Cat# C404010
Chemicals, peptides, and recombinant proteins		
Creatine phosphate	Roche	Cat# 10621722001

Adenosine 5'-triphosphate disodium salt hydrate (ATP)	Sigma-Aldrich	Cat# A3377
Adenosine 5'-[γ-thio] triphosphate tetralithium salt	Roche	Cat# 11162306001
Dpnl	NEB	Cat# R0176S
Gateway BP Clonase II Enzyme Mix	Invitrogen	Cat# 11789013
Gateway LR Clonase II Enzyme Mix	Invitrogen	Cat# 11791019
NEBuilder HiFi DNA Assembly Master Mix	NEB	Cat# E2621S
cOmplete, Mini, EDTA-free Protease Inhibitor Cocktail	Sigma-Aldrich	Cat# 4693159001
Casein fluorescein isothiocyanate from bovine milk (FITC-Casein)	Sigma-Aldrich	Cat# C0528
Creatine kinase	Roche	Cat# 10127566001
Firefly luciferase	Sigma-Aldrich	Cat# L9506
Lysozyme	Sigma-Aldrich	Cat# L6876
Hoechst 33342 stain	Invitrogen	Cat# H3570
Lipofectamine 2000 Transfection Reagent	Invitrogen	Cat# 11668027
VECTASHIELD Antifade Mounting Medium with DAPI	Vector Laboratories	Cat# H-1200-10
DMEM, high glucose, pyruvate	Gibco	Cat# 11995065
Fetal bovine serum	Cytiva	Cat# SH30910.03
Penicillin-streptomycin	Gibco	Cat# 15140122
TeSR Plus medium	STEMCELL Technologies	Cat# 100-0276
HCl	Sigma	Cat# H9892
His-TEV protease	Cupo and Shorter ⁸³	N/A
Hsp104	Jackrel et al. ²⁹	N/A
Hsp104 ^{A503S}	Jackrel et al. ²⁹	N/A
Hsp104 ^{R179D/V}	This paper	N/A
Hsp104 ^{I187F}	Tariq et al. ⁶³	N/A
Hsp104 ^{E190R/K}	This paper	N/A
Hsp104 ^{E190R/K:R419E}	This paper	N/A
Hsp104 ^{E191R:R419E}	This paper	N/A

Hsp104 ^{E192R:R419E}	This paper	N/A
Hsp104 ^{E190R:E191R:R419E}	This paper	N/A
Hsp104 ^{E190R:E192R:R419E}	This paper	N/A
Hsp104 ^{R194E}	Gates et al. ⁵⁹	N/A
Hsp104 ^{E412K}	Gates et al. ⁵⁹	N/A
Hsp104 ^{R194E:E412K}	This paper	N/A
Hsp104 ^{R353E}	Gates et al. ⁵⁹	N/A
Hsp104 ^{E427K}	Gates et al. ⁵⁹	N/A
Hsp104 ^{R353E:E427K}	This paper	N/A
Hsp104 ^{R366E}	Gates et al. ⁵⁹	N/A
Hsp104 ^{D434K}	Gates et al. ⁵⁹	N/A
Hsp104 ^{R366E:D434K}	This paper	N/A
Hsp104 ^{D231R}	This paper	N/A
Hsp104 ^{D232V/R}	This paper	N/A
Hsp104 ^{D233R}	This paper	N/A
Hsp104 ^{K358D}	Mack et al. ³⁰	N/A
Hsp104 ^{E360R}	Tariq et al. ⁶³	N/A
Hsp104 ^{I361K}	This paper	N/A
Hsp104 ^{D408K/V}	This paper	N/A
Hsp104 ^{K410E/L/V}	This paper	N/A
Hsp104 ^{D492R}	This paper	N/A
Hsp104 ^{R495D/E/N/M}	Tariq et al. ⁶³	N/A
Hsp104 ^{R496D}	This paper	N/A
Hsp104 ^{R496V}	Ryan et al. ³⁹	N/A
Hsp104 ^{D484K}	Mack et al. ³⁰	N/A
Hsp104 ^{K480E}	Tariq et al. ⁶³	N/A
Hsp104 ^{K480C/L}	This paper	N/A
Hsp104 ^{K481C/E/L}	This paper	N/A
Hsp104 ^{Y466C/K}	This paper	N/A
Hsp104 ^{E521R/V}	This paper	N/A
Hsp104 ^{M536K}	This paper	N/A
Hsp104 ^{I537A/R}	This paper	N/A
Hsp104 ^{H473F}	This paper	N/A

Hsp104 ^{A531V}	This paper	N/A
Hsp104 ^{R407E}	This paper	N/A
Hsp104 ^{K470D/V}	This paper	N/A
Hsp104 ^{K470Q}	Jackrel et al. ⁵⁸	N/A
Hsp104 ^{D408K/V}	This paper	N/A
Hsp104 ^{L414K}	This paper	N/A
Hsp104 ^{N539L/E/D/G/K}	Jackrel et al. ²⁹	N/A
Hsp104 ^{P411H}	This paper	N/A
Hsp104 ^{E412K}	This paper	N/A
Hsp104 ^{R419E}	Gates et al. ⁵⁹	N/A
GroEL _{trap}	Jackrel et al. ²⁹	N/A
RepA ₁₋₁₅ -GFP	This paper	N/A
Hsc70	Enzo Life Sciences	Cat#ADI-SPP-751-F
DnaJA1	Enzo Life Sciences	Cat#ADI-SPP-405-F
pE-His ₆ -SUMO-Ssa1	Michalska et al. ⁸⁴	N/A
pE-His ₆ -SUMO-Sis1	Michalska et al. ⁸⁴	N/A
pE-His ₆ -SUMO-Ydj1	Michalska et al. ⁸⁴	N/A
pFGET19-Ulp1	Addgene	Plasmid #64697
Luciferase Assay Reagent	Promega	Cat# E1483
ATPase Activity Kit (Colorimetric)	Innova Biosciences	Cat# 601-0120
QuikChange Site-Directed Mutagenesis Kit	Agilent	Cat# 200518
Experimental models: Organisms/strains		
<i>S. cerevisiae</i> : W303aΔ <i>hsp104</i> (<i>MATa</i> , <i>can1-100</i> , <i>his3-11, 15</i> , <i>leu2-3, 112</i> , <i>trp1-1</i> , <i>ura3-1</i> , <i>ade2-1</i> , <i>hsp104::KanMX</i>)	Jackrel et al. ²⁹	N/A

<i>S. cerevisiae</i> : W303aΔhsp104-pAG303GAL-α-syn-YFP-pAG304GAL-α-syn-YFP	Jackrel et al. ²⁹	N/A
<i>S. cerevisiae</i> : W303aΔhsp104-pAG303GAL-FUS	Jackrel et al. ²⁹	N/A
<i>S. cerevisiae</i> : W303aΔhsp104-pAG303GAL-TDP-43	Jackrel et al. ²⁹	N/A
Cell line:		
Human:HeLa	ATCC	Cat#CCL-2;RRID:CVCL_0030
Recombinant DNA		
pAG416GAL-CCDB		
pAG416GAL-Hsp104	Jackrel et al. ²⁹	N/A
pAG416GAL-Hsp104 ^{A503S}	Jackrel et al. ²⁹	N/A
pAG416GAL-Hsp104 ^{R179D/V}	This paper	N/A
pAG416GAL-Hsp104 ^{I187F}	Tariq et al. ⁶³	N/A
pAG416GAL-Hsp104 ^{E190R/K}	This paper	N/A
pAG416GAL-Hsp104 ^{E190R/K:R419E}	This paper	N/A
pAG416GAL-Hsp104 ^{E191R:R419E}	This paper	N/A
pAG416GAL-Hsp104 ^{E192R:R419E}	This paper	N/A
pAG416GAL-Hsp104 ^{E190R:E191R:R419E}	This paper	N/A
pAG416GAL-Hsp104 ^{E190R:E192R:R419E}	This paper	N/A
pAG416GAL-Hsp104 ^{E190R:E191R:E192R:R419E}	This paper	N/A
pAG416GAL-Hsp104 ^{R194E}	Gates et al. ⁵⁹	N/A
pAG416GAL-Hsp104 ^{E412K}	Gates et al. ⁵⁹	N/A
pAG416GAL-Hsp104 ^{R194E:E412K}	This paper	N/A
pAG416GAL-Hsp104 ^{R353E}	Gates et al. ⁵⁹	N/A
pAG416GAL-Hsp104 ^{E427K}	Gates et al. ⁵⁹	N/A
pAG416GAL-Hsp104 ^{R353E:E427K}	This paper	N/A
pAG416GAL-Hsp104 ^{R366E}	Gates et al. ⁵⁹	N/A
pAG416GAL-Hsp104 ^{D434K}	Gates et al. ⁵⁹	N/A
pAG416GAL-Hsp104 ^{R366E:D434K}	This paper	N/A
pAG416GAL-Hsp104 ^{D231R}	This paper	N/A
pAG416GAL-Hsp104 ^{D232V/R}	This paper	N/A

pAG416GAL-Hsp104 ^{D233R}	This paper	N/A
pAG416GAL-Hsp104 ^{K358D}	Mack et al. ³⁰	N/A
pAG416GAL-Hsp104 ^{E360R}	Tariq et al. ⁶³	N/A
pAG416GAL-Hsp104 ^{I361K}	This paper	N/A
pAG416GAL-Hsp104 ^{D408K/V}	This paper	N/A
pAG416GAL-Hsp104 ^{K410E/L/V}	This paper	N/A
pAG416GAL-Hsp104 ^{D492R}	This paper	N/A
pAG416GAL-Hsp104 ^{R495D/E/N/M}	Tariq et al. ⁶³	N/A
pAG416GAL-Hsp104 ^{R496D/V}	This paper	N/A
pAG416GAL-Hsp104 ^{D484K}	Mack et al. ³⁰	N/A
pAG416GAL-Hsp104 ^{K480E}	Tariq et al. ⁶³	N/A
pAG416GAL-Hsp104 ^{K480C/L}	This paper	N/A
pAG416GAL-Hsp104 ^{K481C/E/L}	This paper	N/A
pAG416GAL-Hsp104 ^{Y466C/K}	This paper	N/A
pAG416GAL-Hsp104 ^{E521R/V}	This paper	N/A
pAG416GAL-Hsp104 ^{M536K}	This paper	N/A
pAG416GAL-Hsp104 ^{I537A/R}	This paper	N/A
pAG416GAL-Hsp104 ^{H473F}	This paper	N/A
pAG416GAL-Hsp104 ^{A531V}	This paper	N/A
pAG416GAL-Hsp104 ^{R407E}	This paper	N/A
pAG416GAL-Hsp104 ^{K470D/V}	This paper	N/A
pAG416GAL-Hsp104 ^{K470Q}	Jackrel et al. ⁵⁸	N/A
pAG416GAL-Hsp104 ^{D408K/V}	This paper	N/A
pAG416GAL-Hsp104 ^{L414K}	This paper	N/A
pAG416GAL-Hsp104 ^{N539L/E/D/G/K}	Jackrel et al. ²⁹	N/A
pAG416GAL-Hsp104 ^{P411H}	This paper	N/A
pAG416GAL-Hsp104 ^{E412K}	This paper	N/A
pAG416GAL-Hsp104 ^{R419E}	Gates et al. ⁵⁹	N/A
pNOTAG-Hsp104	Jackrel et al. ²⁹	N/A
pNOTAG-Hsp104 ^{A503S}	Jackrel et al. ²⁹	N/A
pNOTAG-Hsp104 ^{R194E}	Gates et al. ⁵⁹	N/A
pNOTAG-Hsp104 ^{E412K}	Gates et al. ⁵⁹	N/A
pNOTAG-Hsp104 ^{R194E:E412K}	This paper	N/A

pNOTAG-Hsp104 ^{R353E}	Gates et al. ⁵⁹	N/A
pNOTAG-Hsp104 ^{E427K}	Gates et al. ⁵⁹	N/A
pNOTAG-Hsp104 ^{R353E:E427K/R}	This paper	N/A
pNOTAG-Hsp104 ^{R366E}	Gates et al. ⁵⁹	N/A
pNOTAG-Hsp104 ^{D434K}	Gates et al. ⁵⁹	N/A
pNOTAG-Hsp104 ^{R366E:D434K/R}	This paper	N/A
pNOTAG-Hsp104 ^{E360R}	Tariq et al. ⁶³	N/A
pNOTAG-Hsp104 ^{S535E}	Tariq et al. ⁶⁴	N/A
pRS313HSE-ccdB	Gates et al. ⁵⁹	N/A
pRS313HSE--Hsp104 ^{WT}	Gates et al. ⁵⁹	N/A
pRS313HSE--Hsp104 ^{E190K}	This paper	N/A
pRS313HSE--Hsp104 ^{R419E}	This paper	N/A
pRS313HSE -Hsp104 ^{R194E:E412K/R}	This paper	N/A
pRS313HSE -Hsp104 ^{R353E:E427K/R}	This paper	N/A
pRS313HSE -Hsp104 ^{R366E:D434K/R}	This paper	N/A
pTrc99A-GroEL _{trap}	Jackrel et al. ²⁹	N/A
pBAD-RepA ₁₋₁₅ -GFP	Lopez et al. ⁷⁹	N/A
pE-SUMO-Hsp72	This study	N/A
pHis-TEV	Cupo and Shorter ⁸³	N/A
pEGFP-FUS ^{WT}	Fare et al. ⁸⁰	N/A
mCherry2-N1	N/A	AddgeneCat#54563
PMV-Hsp104-mCherry	This study	N/A
PMV- Hsp104 ^{A503S} -mCherry	This study	N/A
PMV- Hsp104 ^{E191R:R419E} -mCherry	This study	N/A
PMV- Hsp104 ^{E360R} -mCherry	This study	N/A
PMV- Hsp104 ^{K481E} -mCherry	This study	N/A
PMV- Hsp104 ^{E535R} -mCherry	This study	N/A
Software and algorithms		N/A
Prism 9	GraphPad	
ImageJ	Rueden et al. ⁸⁵	N/A
PyMOL 4.6.0	Schrodinger, LLC	N/A

Discovery Studio Visualizer	Dassault Systemes Biovia Corp	N/A
-----------------------------	-------------------------------------	-----

584

585 RESOURCE AVAILABILITY

586 *Lead contact*

587 Further information and requests for resources and reagents should be directed to and will be
588 fulfilled by the lead contact, James Shorter (jshorter@penncell.com).

589 *Materials availability*

590 Plasmids newly generated in this study will be made readily available to the scientific
591 community. We will honor requests in a timely fashion. Material transfers will be made with no
592 more restrictive terms than in the Simple Letter Agreement or the Uniform Biological Materials
593 Transfer Agreement and without reach through requirements.

594 *Data and code availability*

595 Any additional information required to reanalyze the data reported in this paper is available from
596 the lead contact upon request.

597 EXPERIMENTAL MODEL AND SUBJECT DETAILS

598 **Yeast strains**

599 Yeast strains used were wild-type W303a (*MATa*, *can1-100*, *his3-11, 15*, *leu2-3, 112*, *trp1-1*,
600 *ura3-1*, *ade2-1*) or the isogenic strain W303a Δ *hsp104*.²⁹ The yeast strains W303a Δ *hsp104*-
601 pAG303GAL- α -syn-YFP-pAG304GAL- α -syn-YFP, W303a Δ *hsp104*-pAG303GAL-FUS, and
602 W303a Δ *hsp104*-pAG303GAL-TDP-43, have been described previously.^{29,36,38} Yeast were
603 grown in rich medium (YPD) or in synthetic media without amino acids used for selection. 2%
604 sugar (dextrose, raffinose, or galactose) was added to synthetic media.

605 **HeLa cell maintenance**

606 Once thawed, HeLa cells were maintained in Dulbecco's modified Eagle's medium (DMEM)
607 containing high glucose, supplied by Gibco. This medium was enriched with 10% fetal bovine
608 serum (FBS) from HyClone and 1% penicillin-streptomycin solution from Gibco. The cells were

609 incubated in a humidified incubator at 37°C at 5% (v/v) CO₂. Cells that pass passage number
610 20 were discarded.

611 **METHOD DETAILS**

612 **Site-directed mutagenesis**

613 Mutations were introduced into Hsp104 through QuikChange site-directed mutagenesis (Agilent)
614 and confirmed by DNA sequencing.

615 **Protein purification**

616 **Hsp104**

617 Hsp104 proteins were purified as previously described with the following modifications.²⁹ Eluate
618 from Affi-Gel Blue Gel was equilibrated to a low-salt buffer Q (~100mM NaCl, 20mM Tris-HCl
619 pH 8.0, 5mM MgCl₂, 0.5mM EDTA and 10% glycerol) and purified via ResourceQ anion
620 exchange chromatography. Buffer Q (20mM TRIS-HCl pH 8.0, 50mM NaCl, 5mM MgCl₂, 0.5mM
621 EDTA, and 10% glycerol) was used as running buffer, and the protein was eluted with a linear
622 gradient of buffer Q+ (20mM Tris-HCl pH 8.0, 1M NaCl, 5mM MgCl₂, 0.5mM EDTA, and 10%
623 glycerol). The eluted protein was buffer-exchanged into high-salt storage buffer (40mM HEPES-
624 KOH pH 7.4, 500mM KCl, 20mM MgCl₂) plus 50% glycerol and 1mM DTT and snap-frozen.

625 **GroEL_{trap}**

626 pTrc99A-GroEL_{trap} was transformed into DH5α competent *E. coli* cells (Thermo Fisher). Cells
627 were grown in 2xYT medium with appropriate antibiotics at 37°C with shaking until OD₆₀₀
628 reached ~0.4-0.6. Protein overexpression was induced with 1mM IPTG, and cells were grown at
629 37°C until OD₆₀₀~2.0. Cells were harvested by spinning (4,658g, 4°C, 15min) and pellet was
630 resuspended in 50mM sodium phosphate buffer and centrifuged (4,658g, 4°C, 15min). The
631 pellet fraction was resuspended in low-salt buffer (50mM Tris-HCl pH 7.5, 1mM EDTA, 1mM
632 DTT, 50mM NaCl) and 10mg lysozyme per g cell pellet. Sample was stirred gently for 5min,
633 lysed through sonication, and centrifuged (30,996g, 4°C, 30min). Clarified lysate was loaded
634 onto HiTrap Q HP column (GE Healthcare) and eluted through salt gradient using low-salt buffer
635 (as described above) and high-salt buffer (50mM Tris-HCl pH 7.5, 1mM EDTA, 1mM DTT,
636 500mM NaCl).⁸⁶ Collected fractions were exchanged into the following TKME-100 buffer: 20mM
637 Tris-HCl pH 7.5, 100mM KCl, 10mM MgCl₂, 0.1mM EDTA, 5mM DTT, 10% glycerol, and
638 0.005% Triton X-100, and snap-frozen.

639 **RepA₁₋₁₅-GFP**

640 pBAD-RepA₁₋₁₅-GFP was transformed into BL21 (DE3)-RIL cells. Cells were inoculated in 2xYT
641 medium with appropriate antibiotics at 37°C with shaking until OD₆₀₀ reached ~0.6-0.8. Protein
642 overexpression was induced with 1mM IPTG, and cells were grown at 30°C for 4h. Cells were
643 harvested by spinning (4,658g, 4°C, 25min) and pellet was resuspended in 40mM HEPES-KOH
644 pH 7.4 plus 2mM 2-Mercaptoethanol (BME) and EDTA-free protease inhibitors. Cells were lysed
645 using a sonicator and centrifuged (30,996g, 4°C, 20min). The resulting pellet was washed twice
646 with HM buffer (40mM HEPES-KOH pH 7.4, 20mM MgCl₂) plus 2mM BME. After each wash,
647 cells were centrifuged (30,996g, 4°C, 20min). The pellet fraction was then resuspended in buffer
648 containing 8M urea, 40mM Tris-HCl pH 6.8, 500mM NaCl, 10% glycerol (v/v) and agitated
649 slowly overnight at 25°C. The solubilized pellet was then centrifuged (30,996g, 25°C, 20min)
650 and the supernatant was collected. The supernatant fraction was incubated with Ni-NTA beads
651 (HisPur™ Ni-NTA Resin, Thermo Scientific) pre-equilibrated in buffer containing 8M urea, 40mM
652 Tris pH 6.8, 500mM NaCl, 10% glycerol (v/v) for 2h on a spinning wheel at 25°C at the lowest
653 speed. The Ni-NTA beads were then washed 5 times with buffer containing 8M urea, 40mM
654 Tris-HCl pH 6.8, 500mM NaCl, 20mM imidazole, 10% glycerol (v/v) and then washed 5 times
655 with buffer containing 8M urea, 40mM Tris-HCl pH 6.8, 500mM NaCl, 40mM imidazole, 10%
656 glycerol (v/v). The Ni-NTA beads were then eluted with buffer containing 8M urea, 40mM Tris-
657 HCl pH 6.8, 500mM NaCl, 500mM imidazole, 10% glycerol (v/v). The eluate was dialyzed
658 overnight into buffer containing 40mM HEPES-KOH pH 7.4, 20mM imidazole, 150mM KCl, 2mM
659 BME, 10% glycerol (v/v) at 4°C and re-loaded onto a Ni-NTA column (HisTrap™ HP, GE
660 Healthcare). An imidazole gradient was applied (from 20mM to 500mM) over 20CV in buffer
661 containing 40mM HEPES-KOH pH 7.4, 20mM imidazole, 150mM KCl, 2mM BME, 10% glycerol
662 (v/v). The purity of eluted fractions was assessed using SDS-PAGE. Collected fractions were
663 buffer-exchanged into HKM-150 buffer (40mM HEPES-KOH pH 7.4, 150mM KCl, 20mM MgCl₂)
664 plus 2 mM BME and 10% glycerol (v/v) and snap-frozen.

665 **Hsp70 and Hsp40**

666 Hsc70 and DnaJA1 were from Enzo Life Sciences. Ssa1, Ydj1 and Sis1 were purified as
667 described.⁸⁴

668 **ATPase assay**

669 0.25 μ M (monomeric) Hsp104 was incubated with ATP (1mM) for 5min at 25°C in luciferase-
670 refolding buffer (LRB150: 25mM HEPES-KOH pH 7.4, 150mM KAOc, 10mM MgAOc, 2 mM 2-
671 Mercaptoethanol). The final reaction buffer contained < 0.3 % of HKM-500 buffer (stock of
672 Hsp104 is >100 μ M). ATPase activity was evaluated by the release of inorganic phosphate,
673 which was measured using a malachite green phosphate detection kit (Innova Biosciences).
674 Background hydrolysis at time zero was subtracted.

675 **Luciferase disaggregation and reactivation assay**

676 Aggregated luciferase (100nM, monomer concentration) was incubated with Hsp104 or Hsp104
677 variants (1 μ M monomer), ATP (5mM), and an ATP regeneration system (10mM creatine
678 phosphate, 0.25 μ M creatine kinase) in the presence or absence of additional chaperones
679 Hsp70 (Hsc70 or Ssa1, various concentrations as indicated in the figure) and Hsp40 (Ydj1,
680 DnaJA1, or Sis1), for 90min at 25°C in LRB. The final reaction buffer contained less than 1% of
681 HKM-500 buffer. After 90min, luciferase activity was measured with a luciferase assay reagent
682 (Promega). Recovered luminescence was measured using a Tecan Infinite M1000 or Spark
683 plate reader.

684 **Luciferase refolding assay**

685 Native luciferase (10 μ M) in 6M urea was incubated on ice for 5 min. The sample was then
686 diluted to a final luciferase concentration of 1, 2, 10 or 20 nM in to LRB150 with an ATP
687 regeneration system (10mM creatine phosphate, 0.25 μ M creatine kinase), at the indicated
688 Hsp40 (Ydj1 or Sis1) concentration. The sample was then incubated for 90min at 25°C. After
689 90min, luciferase activity was measured with a luciferase assay reagent (Promega). Recovered
690 luminescence was measured using a Tecan Infinite M1000 or Spark plate reader.

691 To check luciferase spontaneous refolding, native luciferase (10 μ M) in 6M urea was incubated
692 on ice for 5 min. The sample was then diluted to a final luciferase concentration of 1, 2, 10, or
693 20 nM into LRB150 with ARS. The activity of luciferase was measured at time of dilution (0 min)
694 and after incubated for 90 min at 25°C as described above.

695 **Yeast plasmids**

696 Hsp104 variants were under control of a galactose-inducible promoter on pAG416GAL
697 plasmids. In thermotolerance assays, Hsp104 expression was induced by 30min incubation in
698 37°C through a heat inducible HSE promoter on pRS313HSE plasmids.

699 **Thermotolerance assay**

700 Hsp104 variants under the HSE promoter were transformed into *W303aΔhsp104* yeast. Yeast
701 cultures were grown to saturation overnight at 30°C in glucose dropout media. Cultures were
702 normalized to OD₆₀₀ = 0.3 and grown in glucose dropout media at 30°C for at least 4h, after
703 which the equivalent of 6 ml culture with an OD₆₀₀ = 0.6 was grown at 37°C for 30 min (if
704 assessing Hsp104 expression, samples would be harvested at this stage for western blot as
705 described above). Cultures were then heat-shocked at 50°C in 1.5ml Eppendorf tubes in an
706 Eppendorf Thermomixer for 30min and incubated on ice for 2min. Cultures were diluted
707 appropriately, plated on glucose dropout media, and incubated at 30°C. After 2-3 days, colonies
708 were counted using an aCOLyte colony counter and software (Synbiosis). Spotting result
709 presented in Figure 3B was quantified using ImageJ as described in the quantification and
710 statistical analysis section.

711 **Yeast transformation and spotting assays**

712 Plasmids containing Hsp104 variants were transformed into yeast using a standard lithium
713 acetate and polyethylene glycol procedure.⁸⁷ For spotting assays, yeast cultures were grown to
714 saturation overnight at 30°C in dropout media containing raffinose. Raffinose cultures were then
715 normalized to an OD₆₀₀=2. Five-fold serial dilution was performed on sterile 96-well plates and
716 spotted onto glucose and galactose plates using a 96-bolt replicator tool. Plates were grown at
717 30°C for 3 days and imaged at both day 2 and day 3.

718 **Western blotting**

719 For yeast Western blotting, Hsp104 variants transformed into appropriate yeast strains were
720 grown to saturation overnight at 30°C in dropout media containing raffinose. Cultures were
721 normalized to OD₆₀₀ = 0.3 and grown in galactose dropout media at 30°C to induce Hsp104 and
722 disease substrate expression (TDP-43 and FUS cultures induced for 5h). Galactose cultures
723 were then normalized according to OD₆₀₀ and the equivalent of 6ml culture with an OD₆₀₀ = 0.6
724 were harvested by centrifugation. Media was aspirated, and the cell pellets were resuspended
725 in 0.1M NaOH and incubated at room temperature for 5min. Cells were pelleted again by
726 centrifugation, supernatant removed, and pellet was resuspended in 100μL 1X SDS sample
727 buffer and boiled for 4-5min. Samples were separated via SDS-PAGE (4-20% gradient, Bio-
728 Rad) and transferred to a PVDF membrane (Millipore) using a Trans-Blot SD Semi-Dry Transfer
729 Cell (Bio-Rad). Membranes were blocked for at least 1h at room temperature and then

730 incubated with primary antibodies (rabbit anti-Hsp104 polyclonal (Enzo Life Sciences); rabbit
731 anti-FUS polyclonal (Bethyl Laboratories); rabbit anti-TDP-43 polyclonal (Proteintech); rabbit
732 anti-GFP polyclonal (Sigma-Aldrich); mouse anti-PGK1 monoclonal (Thermo Fisher) at 4°C
733 overnight. Membranes were washed multiple times with PBS-T, incubated with secondary
734 antibodies (goat anti-mouse and goat anti-rabbit, LI-COR) for 1h at room temperature, and
735 washed again multiple times with PBS-T (final wash with PBS). Membranes were imaged using
736 a LI-COR Odyssey FC Imaging system.

737 **Toxicity spotting assay**

738 pAG416GAL plasmids containing Hsp104 variants were transformed into W303aΔ*hsp104* yeast.
739 Yeast cultures were grown to saturation overnight at 30°C in dropout media containing raffinose.
740 Raffinose cultures were then normalized according to OD₆₀₀ and five-fold serial diluted. The
741 cultures were spotted onto two sets of glucose and galactose plates using a 96-bolt replicator
742 tool. One set of plates was grown at 30°C, and the other at 37°C, for three days and imaged
743 subsequently at day 2 and day 3.

744 **RepA₁₋₁₅-GFP unfoldase assay**

745 RepA₁₋₁₅-GFP (0.7μM) was incubated with Hsp104 or Hsp104 variants (6μM, monomeric), ATP
746 (4mM), ARS (20mM creatine phosphate, 0.06μg/μl creatine kinase). GroEL_{trap} (2.5μM
747 tetradecamer) was included to prevent refolding of unfolded RepA₁₋₁₅-GFP. Hsp104 variants
748 were buffer-exchanged into TKME-100 buffer at 25°C. Reactions were assembled on ice in
749 TKME-100 buffer plus 20μg/ml BSA. RepA₁₋₁₅-GFP unfolding was measured by fluorescence
750 (excitation 395nm, emission 510nm) using a Tecan Safire², which was heated to 30°C prior to
751 reading.

752 **Codon-optimized Hsp104 plasmid for human cell expression:**

753 The codon optimized Hsp104 plasmid for human cell expression were purchased through Twist
754 by two fragments with 20nt overhangs to insert into mCherry2-N1 plasmid using Gibson
755 Assembly. The mCherry-N1 plasmid was linearized using AgeI restriction enzyme. For
756 mCherry-tagged Hsp104 variants, mCherry is located at the C-terminal end of Hsp104. The
757 following Hsp104 sequence was inserted on the N-terminal site of mCherry separated by a
758 glycine-serine linker (Gly-Gly-Ser-Gly-Gly-Gly-Ser-Gly-Gly).

759 ATGAATGACCAGACGCAGTTCACGGAGCGCGCTCACCATACTCACACTTGACAAAAA
760 CTTGCGTCTGATCACCAGCACCCGCAGCTCCAACCCATCCATATCTTGGCAGCGTTCATTG

761 A G A C T C C A G A A G A C G G G T C A G T A C C C T A T C T G C A G A A T C T G A T A G A G A A G G G A A G G T A T G
762 A T T A C G A T T T G T T T A A A A A G G T C G T T A A T C G A A A C T T G G T A C G G A T C C C C C A A C A A C A G C C A
763 G C T C C G G C T G A G A T A A C T C C G A G T T A T G C T C T C G G A A A G G T A C T G C A G G A T G C A G C T A A G
764 A T T C A G A A G C A G C A G A A A G A T T C A T T T A T C G C C C A A G A T C A T A T T C T C T T C G C T C T G T T C A A
765 C G A C T C A T C C A T T C A A C A G A T C T T C A A G G A G G C T C A G G T G G A C A T A G A A G C T A T C A A G C A G
766 C A G G C C T T G G A G T T G C G C G G G A A C A C G A G A A T T G A T T C C C G C G G C G C A G A T A C T A A T A C A
767 C C T C T G G A A T A T C T T T C T A A A T A T G C A A T A G A T A T G A C G G A G C A G G C C A G A C A G G G C A A A T
768 T G G A T C C A G T G A T A G G G C G A G A G G A G A T T C G C T C A A C T A T T C G A G T C C T T G C T C G A A
769 G A A T A A A A G C A A C C C A T G T C T G A T T G G T G A A C C G G G A A T T G G T A A G A C T G C A A T C A T C G A
770 A G G C G T T G C T C A G A G A A T C A T C G A T G A C G A T G T G C C A A C C A T A C T T C A G G G G G C G A A G C T
771 G T T T A G T C T C G A T C T T G C T G C C C T T A C C G C T G G T G C A A A G T A C A A A G G C G A C T T T G A A G A G
772 C G G T T T A A G G G T G T C C T C A A G G A A A T C G A G G A A T C A A A G A C C C T T A T C G T G C T T T T C A T A G
773 A C G A G A T T C A T A T G T T G A T G G G G A A T G G G A A A G A T G A T G C G G C T A A C A T A C T C A A G C C T G C
774 G C T C T C A C G A G G A C A G C T C A A G G T T A T T G G C G C T A C T A C C A A C A A C G A G T A C A G A T C A A T A
775 G T T G A A A A G G A C G G C G C G T T C G A A C G G C G G T T T C A A A A A A T A G A A G T A G C T G A G C C G A G C
776 G T G A G A C A G A C T G T C G C C A T A T T G A G G G G T C T C C A G C C T A A G T A C G A A A T C C A T C A C G G C
777 G T G C G G A T C C T G G A C T C A G C A C T G G T T A C A G C G G C G C A G T T G G C G A A A C G G T A T C T T C C C
778 T A C C G C A G G T T G C C C G A C T C T G C T C T T G A C T T G G T A G A C A T A A G T T G T G C G G G C G T G G C A
779 G T T G C A A G A G A C T C C A A C C T G A A G A A T T G G A C T C C A A G A G C G A C A A C T C C A A C T G A T C C
780 A G G T C G A G A T T A A A G C G T T G G A G C G C G A C G A A G A C G C G G A C T C T A C T A C T A A G G A C C G G C
781 T T A A A C T T G C T C G A C A G A A G G A A G C G T C C C T C C A G G A G G A A C T C G A G C C T T T G A G G C A G C
782 G A T A C A A C G A G G A A A A C A C G G A C A T G A G G A A C T G A C C C A A G C T A A G A A A A G C T C G A C G
783 A G C T T G A G A A C A A A G C C C T C G A T G C G G A G A G A G A T A T G A T A C T G C T A C T G C T G C T G A C C
784 T G A G A T A C T T T G C T A T C C C T G A T A T T A A G A A A C A G A T C G A A A A G C T G G A G G A T C A G G T T G C
785 T G A A G A A G A A A G A C G A G C C G G A G C G A A T T C A A T G A T A C A G A A C G T C G T T G A T A G T G A T A C
786 G A T A T C C G A A A C A G C C G C G C G A C T T A C T G G A A T A C C G G T T A A A A G C T C T C A G A G T C T G A G
787 A A T G A A A A A C T C A T T C A C A T G G A A C G C G A T C T C A G T T C A G A A G T T G T C G G T C A G A T G G A C G
788 C C A T T A A G G C A G T A T C C A A C G C T G T A C G A C T T T C C A G G T C T G G C C T T G C A A A T C C G C G C C A
789 A C C T G C T A G C T T T C T T T T C C T T G G C C T G T C A G G G T C C G G A A A A C A G A A C T G G C T A A G A A G
790 G T T G C A G G G T T T C T G T T T A A C G A T G A A G A T A T G A T G A T T A G A G T A G A C T G C T C T G A A C T G T C
791 C G A G A A A T A C G C C G T G A G T A A A T T G C T C G G A A C C A C T G C C G G A T A T G T T G G A T A T G A C G A A
792 G G C G G A T T C C T C A C A A A T C A G C T G C A G T A C A A C C A T A C A G C G T C C T T T T G T T C G A T G A A G
793 T C G A G A A G G C T C A C C C A G A C G T T C T G A C T G T T A T G C T C C A G A T G C T T G A T G A T G G G A G G A T
794 T A C T T C T G G T C A A G G A A A G A C C A T C G A T T G C A G C A A C T G T A T T G T A A T C A T G A C C A G T A A T T

795 TGGGTGCTGAATTCATCAACAGTCAGCAGGGTTCAAAAATCCAAGAATCCACTAAAAACCT
796 GGTTATGGGGGCAGTTCGGCAACACTTTCGCCCTGAATTTCTTAATCGAATCTCATCCATC
797 GTGATATTCAACAAGCTCAGTCGCAAGGCAATCCATAAAATTGTGGACATAAGACTCAAAG
798 AGATAGAAGAAAGGTTTGAACAGAACGATAAGCATTACAAGCTTAATCTGACACAGGAGGC
799 AAAGGACTTCCTCGCGAAGTACGGGTATAGCGACGACATGGGTGCTAGACCGCTTAATCG
800 CTTGATTCAAAATGAGATCCTCAACAAGCTGGCTCTTAGGATACTGAAAAACGAGATCAAG
801 GACAAAGAGACTGTGAATGTAGTGTTGAAAAGGGAAAATCCCGAGATGAAAATGTACCGG
802 AAGAGGCCGAGGAATGCCTTGAAGTACTTCCAAACCATGAGGCAACCATCGGTGCTGATA
803 CCCTCGGTGATGATGATAACGAAGATTCAATGGAAATCGACGACGACCTCGAC

804 **HeLa cell culture and transfections**

805 HeLa cells were cultured in Dulbecco's Modified Eagle Medium (DMEM) with high glucose,
806 supplied by Gibco, which was enriched with 10% fetal bovine serum (FBS) from HyClone and
807 1% penicillin-streptomycin solution from Gibco. The cells were seeded into 6-well plates at a
808 density of $2\text{--}2.5 \times 10^5$ cells per plate, 24h prior to the transfection. The transfection was carried
809 out with 1.5 μ g of total DNA mixed with 4.5 μ l of Lipofectamine 2000 reagent (Invitrogen). Four
810 hours post-transfection, the medium was replaced with the standard growth medium to continue
811 cell maintenance. 24h after the transfection, the cells were collected for analysis by microscopy
812 or Western blotting.

813 In the microscopy experiments, the colocalization of proteins was assessed manually. At least
814 500 cells per experiment sample were analyzed across four separate trials. The statistical
815 analysis was conducted using a one-way ANOVA with Dunnett's test, with the calculations
816 performed using GraphPad Prism Software.

817 **Western blotting for HeLa cell experiment**

818 For HeLa cells, $\sim 2\text{--}2.5 \times 10^5$ cells were seeded and transfected with GFP-tagged FUS and either
819 mCherry-tagged Hsp104 variants or an empty vector expressing mCherry. After 24h, cells were
820 washed once with PBS, then resuspended in RIPA lysis buffer (150 mM NaCl, 1% Triton X-100,
821 1% sodium deoxycholate, 0.1% SDS, 25mM Tris–HCl pH 7.6) supplemented with protease
822 inhibitors and 1 mM PMSF. Cells were then sonicated and centrifuged at 4°C for 10min at
823 10,000g, and the cell lysate was mixed with 1 \times SDS-PAGE sample buffer.

824 The samples were then boiled and separated by SDS-PAGE (4–20% gradient, Bio-Rad) and
825 transferred to a PVDF membrane. The following primary antibodies were used: rabbit anti-GFP

826 polyclonal (Sigma-Aldrich) for induced GFP-FUS expression, anti-alpha Tubulin monoclonal
827 (Abcam: ab184970 for yeast; ab6160 for human cells), anti-mCherry polyclonal (Abcam). Three
828 fluorescently labeled secondary antibodies were used: anti-rabbit (Li-Cor), anti-rat (Li-Cor), and
829 anti-mouse (Li-Cor). Blots were imaged using a LI-COR Odyssey FC Imaging system.

830 **Fluorescence microscopy**

831 For HeLa cell microscopy, transfected HeLa cells were fixed with 2% formaldehyde for 30 min at
832 room temperature, followed by treatment with Triton X-100 for 6 min to permeabilize cells.
833 Coverslips were then assembled using VECTASHIELD Antifade Mounting Medium with DAPI
834 (Vector Laboratories) and sealed before imaging. Images were taken at 100× magnification
835 using the EVOS M5000 Imaging System (ThermoFisher) and processed using ImageJ. At least
836 100 cells were counted for each condition across four independent trials.

837 **QUANTIFICATION AND STATISTICAL ANALYSIS**

838 The Absolute IC₅₀ model in GraphPad was used to fit the dose-dependent luciferase
839 reactivation isotherms as a function of Ssa1 or Sis1 concentrations.

840 $Fifty = (Top + Baseline) / 2$

841 $Y = Bottom + (Top - Bottom) / (1 + ((Top - Bottom) / (Fifty - Bottom) - 1) * (AbsoluteIC_{50} / X)^{HillSlope})$

842

843 The Bell-shaped dose-response model in GraphPad was used to fit the dose-dependent
844 luciferase reactivation isotherms as a function of Ydj1 concentrations.

845 $Span1 = Plateau1 - Dip$

846 $Span2 = Plateau2 - Dip$

847 $Section1 = Span1 / (1 + (EC_{50_1} / X)^{nH1})$

848 $Section2 = Span2 / (1 + (X / EC_{50_2})^{nH2})$

849 $Y = Dip + Section1 + Section2$

850 Here, X is Ssa1, Sis1 or Ydj1 concentration, and Y is the level of reactivated Luciferase in an
851 arbitrary unit.

852 Quantification is as described in the figure legends. Statistical analyses were performed using
853 the GraphPad Prism (GraphPad Software, Inc.; La Jolla, CA, USA) as described in figure
854 legends.

855 **Thermotolerance spotting assay quantification**

856 The spotting images were opened in imageJ. The image type was changed to 8-bit, and applied
857 background subtraction by choosing 'subtract background' under the 'Process' tab. The image

858 was then converted to binary images by choosing 'Binary' under the 'Process' tab. The density
859 of each spot was then quantified, as D_1 for the first spot, and D_2 for the second spot, etc. For
860 each sample, only the first four spots (5-fold dilution serial) are included for this analysis. The
861 dilution factor was corrected to account for sum of the density (D_{Sum}) for each sample as shown
862 below:

863
$$D_{\text{Sum}} = D_1 + 5 \cdot D_2 + 25 \cdot D_3 + 125 \cdot D_4$$

864 The D_{Sum} of each Hsp104 variant was then normalized to D_{Sum} of Hsp104 for each replicate.

865 **Acknowledgements**

866 We thank Zarin Tabassum, Zhuoyi Chen, and Sabrina Lin for feedback on the manuscript. This
867 work was supported by an Alzheimer's Association Research Fellowship, a Warren Alpert
868 Foundation Distinguished Scholars Fellowship, and a Mildred Cohn Distinguished Postdoctoral
869 Award (J.L.), a Blavatnik Family Foundation Fellowship (E.C.), and NIH grants: T32GM008076
870 (E.C.), R01GM110001 (D.R.S), and R01GM099836 (J.S.).

871

872 **Author contributions**

873 Conceptualization, J.L., D.R.S. & J.S.; Methodology, J.L., E.C., & J.S.; Validation, J.L., P.J.C.,
874 C.W.G., & N.M.K.; Formal analysis, J.L; Investigation, J.L., P.J.C., C.W.G., & N.M.K.; Resources,
875 J.L., P.J.C., C.W.G., N.M.K., E.C., S.N.G., A.L.Y., A.N.R., D.R.S., & J.S.; Data curation, J.L.;
876 Writing–original draft, J.L., & J.S.; Writing–review and editing, J.L., P.J.C., C.W.G., N.M.K., E.C.,
877 S.N.G., A.L.Y., A.N.R., D.R.S., & J.S.; Visualization, J.L., D.R.S. & J.S.; Supervision, J.L., D.R.S.,
878 & J.S.; Project administration, J.L., D.R.S., & J.S.; Funding acquisition, J.L., E.C., D.R.S., & J.S.

879

880 **Declarations of interests**

881 The authors have no conflicts, except for: J.S. is a consultant for Dewpoint Therapeutics, ADRx,
882 and Neumora Therapeutics. J.S. is a shareholder and advisor at Confluence Therapeutics.

883

884

885 **References**

- 886 1. Englander, S.W. (2023). HX and Me: Understanding Allostery, Folding, and Protein
887 Machines. *Annu Rev Biophys* 52, 1-18. 10.1146/annurev-biophys-062122-093517.
- 888 2. Labbadia, J., and Morimoto, R.I. (2015). The biology of proteostasis in aging and
889 disease. *Annu Rev Biochem* 84, 435-464. 10.1146/annurev-biochem-060614-033955.
- 890 3. Lopez-Otin, C., Blasco, M.A., Partridge, L., Serrano, M., and Kroemer, G. (2013). The
891 Hallmarks of Aging. *Cell* 153, 1194-1217. 10.1016/j.cell.2013.05.039.
- 892 4. Eisele, Y.S., Monteiro, C., Fearn, C., Encalada, S.E., Wiseman, R.L., Powers, E.T., and
893 Kelly, J.W. (2015). Targeting protein aggregation for the treatment of degenerative
894 diseases. *Nat Rev Drug Discov* 14, 759-780. 10.1038/nrd4593.
- 895 5. Fare, C.M., and Shorter, J. (2021). (Dis)Solving the problem of aberrant protein states.
896 *Dis Model Mech* 14. 10.1242/dmm.048983.
- 897 6. Balch, W.E., Morimoto, R.I., Dillin, A., and Kelly, J.W. (2008). Adapting proteostasis for
898 disease intervention. *Science* 319, 916-919. 10.1126/science.1141448.
- 899 7. Chuang, E., Hori, A.M., Hesketh, C.D., and Shorter, J. (2018). Amyloid assembly and
900 disassembly. *J Cell Sci* 131. 10.1242/jcs.189928.
- 901 8. Scheres, S.H.W., Ryskeldi-Falcon, B., and Goedert, M. (2023). Molecular pathology of
902 neurodegenerative diseases by cryo-EM of amyloids. *Nature* 621, 701-710.
903 10.1038/s41586-023-06437-2.
- 904 9. Huang, E.J., Zhang, J., Geser, F., Trojanowski, J.Q., Strober, J.B., Dickson, D.W.,
905 Brown, R.H., Jr., Shapiro, B.E., and Lomen-Hoerth, C. (2010). Extensive FUS-
906 immunoreactive pathology in juvenile amyotrophic lateral sclerosis with basophilic
907 inclusions. *Brain Pathol* 20, 1069-1076. 10.1111/j.1750-3639.2010.00413.x.
- 908 10. Portz, B., Lee, B.L., and Shorter, J. (2021). FUS and TDP-43 Phases in Health and
909 Disease. *Trends Biochem Sci* 46, 550-563. 10.1016/j.tibs.2020.12.005.
- 910 11. Shorter, J. (2008). Hsp104: a weapon to combat diverse neurodegenerative disorders.
911 *Neurosignals* 16, 63-74. 10.1159/000109760.

- 912 12. Erjavec, N., Larsson, L., Grantham, J., and Nystrom, T. (2007). Accelerated aging and
913 failure to segregate damaged proteins in Sir2 mutants can be suppressed by
914 overproducing the protein aggregation-remodeling factor Hsp104p. *Genes Dev* 21,
915 2410-2421. 10.1101/gad.439307.
- 916 13. Shorter, J., and Southworth, D.R. (2019). Spiraling in Control: Structures and
917 Mechanisms of the Hsp104 Disaggregase. *Cold Spring Harb Perspect Biol* 11.
918 10.1101/cshperspect.a034033.
- 919 14. Lin, J., Shorter, J., and Lucius, A.L. (2022). AAA+ proteins: one motor, multiple ways to
920 work. *Biochem Soc Trans* 50, 895-906. 10.1042/BST20200350.
- 921 15. Glover, J.R., and Lindquist, S. (1998). Hsp104, Hsp70, and Hsp40: a novel chaperone
922 system that rescues previously aggregated proteins. *Cell* 94, 73-82. S0092-
923 8674(00)81223-4 [pii].
- 924 16. Lo Bianco, C., Shorter, J., Regulier, E., Lashuel, H., Iwatsubo, T., Lindquist, S., and
925 Aebischer, P. (2008). Hsp104 antagonizes alpha-synuclein aggregation and reduces
926 dopaminergic degeneration in a rat model of Parkinson disease. *J Clin Invest* 118, 3087-
927 3097. 10.1172/JCI35781.
- 928 17. Shorter, J., and Lindquist, S. (2004). Hsp104 catalyzes formation and elimination of self-
929 replicating Sup35 prion conformers. *Science* 304, 1793-1797. 10.1126/science.1098007.
- 930 18. DeSantis, M.E., Leung, E.H., Sweeny, E.A., Jackrel, M.E., Cushman-Nick, M., Neuhaus-
931 Follini, A., Vashist, S., Sochor, M.A., Knight, M.N., and Shorter, J. (2012). Operational
932 plasticity enables hsp104 to disaggregate diverse amyloid and nonamyloid clients. *Cell*
933 151, 778-793. 10.1016/j.cell.2012.09.038.
- 934 19. Yoo, H., Bard, J.A.M., Pilipenko, E.V., and Drummond, D.A. (2022). Chaperones directly
935 and efficiently disperse stress-triggered biomolecular condensates. *Mol Cell* 82, 741-755
936 e711. 10.1016/j.molcel.2022.01.005.
- 937 20. Tomaszewski, A., Wang, R., Sandoval, E., Zhu, J., Liu, J., and Li, R. (2023). Solid-to-
938 liquid phase transition in the dissolution of cytosolic misfolded-protein aggregates.
939 *iScience* 26. 10.1016/j.isci.2023.108334.

- 940 21. Vashist, S., Cushman, M., and Shorter, J. (2010). Applying Hsp104 to protein-misfolding
941 disorders. *Biochem Cell Biol* 88, 1-13. 10.1139/o09-121.
- 942 22. Erives, A.J., and Fassler, J.S. (2015). Metabolic and chaperone gene loss marks the
943 origin of animals: evidence for Hsp104 and Hsp78 chaperones sharing mitochondrial
944 enzymes as clients. *PLoS One* 10, e0117192. 10.1371/journal.pone.0117192.
- 945 23. Cupo, R.R., Rizo, A.N., Braun, G.A., Tse, E., Chuang, E., Gupta, K., Southworth, D.R.,
946 and Shorter, J. (2022). Unique structural features govern the activity of a human
947 mitochondrial AAA+ disaggregase, Skd3. *Cell Rep* 40, 111408.
948 10.1016/j.celrep.2022.111408.
- 949 24. Cupo, R.R., and Shorter, J. (2020). Skd3 (human ClpB) is a potent mitochondrial protein
950 disaggregase that is inactivated by 3-methylglutaconic aciduria-linked mutations. *Elife* 9.
951 10.7554/eLife.55279.
- 952 25. Warren, J.T., Cupo, R.R., Wattanasirakul, P., Spencer, D.H., Locke, A.E., Makaryan, V.,
953 Bolyard, A.A., Kelley, M.L., Kingston, N.L., Shorter, J., et al. (2022). Heterozygous
954 variants of CLPB are a cause of severe congenital neutropenia. *Blood* 139, 779-791.
955 10.1182/blood.2021010762.
- 956 26. Cupo, R.R., and Shorter, J. Decoding Skd3 (Human CLPB): a Mitochondrial Protein
957 Disaggregase Critical for Human Health. *Isr. J. Chem.* *n/a*, e202300153.
958 10.1002/ijch.202300153.
- 959 27. Darwich, N.F., Phan, J.M., Kim, B., Suh, E., Papatriantafyllou, J.D., Changolkar, L.,
960 Nguyen, A.T., O'Rourke, C.M., He, Z., Porta, S., et al. (2020). Autosomal dominant VCP
961 hypomorph mutation impairs disaggregation of PHF-tau. *Science* 370.
962 10.1126/science.aay8826.
- 963 28. Cushman-Nick, M., Bonini, N.M., and Shorter, J. (2013). Hsp104 suppresses
964 polyglutamine-induced degeneration post onset in a drosophila MJD/SCA3 model. *PLoS*
965 *Genet* 9, e1003781. 10.1371/journal.pgen.1003781.
- 966 29. Jackrel, M.E., DeSantis, M.E., Martinez, B.A., Castellano, L.M., Stewart, R.M., Caldwell,
967 K.A., Caldwell, G.A., and Shorter, J. (2014). Potentiated Hsp104 variants antagonize
968 diverse proteotoxic misfolding events. *Cell* 156, 170-182. 10.1016/j.cell.2013.11.047.

- 969 30. Mack, K.L., Kim, H., Barbieri, E.M., Lin, J., Braganza, S., Jackrel, M.E., DeNizio, J.E.,
970 Yan, X., Chuang, E., Tariq, A., et al. (2023). Tuning Hsp104 specificity to selectively
971 detoxify alpha-synuclein. *Mol Cell* 83, 3314-3332 e3319. 10.1016/j.molcel.2023.07.029.
- 972 31. March, Z.M., Sweeney, K., Kim, H., Yan, X., Castellano, L.M., Jackrel, M.E., Lin, J.,
973 Chuang, E., Gomes, E., Willicott, C.W., et al. (2020). Therapeutic genetic variation
974 revealed in diverse Hsp104 homologs. *Elife* 9. 10.7554/eLife.57457.
- 975 32. Perrin, V., Regulier, E., Abbas-Terki, T., Hassig, R., Brouillet, E., Aebischer, P., Luthi-
976 Carter, R., and Deglon, N. (2007). Neuroprotection by Hsp104 and Hsp27 in lentiviral-
977 based rat models of Huntington's disease. *Mol Ther* 15, 903-911.
978 10.1038/mt.sj.6300141.
- 979 33. Bao, Y.P., Cook, L.J., O'Donovan, D., Uyama, E., and Rubinsztein, D.C. (2002).
980 Mammalian, yeast, bacterial, and chemical chaperones reduce aggregate formation and
981 death in a cell model of oculopharyngeal muscular dystrophy. *J Biol Chem* 277, 12263-
982 12269. 10.1074/jbc.M109633200.
- 983 34. Carmichael, J., Chatellier, J., Woolfson, A., Milstein, C., Fersht, A.R., and Rubinsztein,
984 D.C. (2000). Bacterial and yeast chaperones reduce both aggregate formation and cell
985 death in mammalian cell models of Huntington's disease. *Proc Natl Acad Sci U S A* 97,
986 9701-9705. 10.1073/pnas.170280697.
- 987 35. Vacher, C., Garcia-Oroz, L., and Rubinsztein, D.C. (2005). Overexpression of yeast
988 hsp104 reduces polyglutamine aggregation and prolongs survival of a transgenic mouse
989 model of Huntington's disease. *Hum Mol Genet* 14, 3425-3433. 10.1093/hmg/ddi372.
- 990 36. Jackrel, M.E., and Shorter, J. (2014). Potentiated Hsp104 variants suppress toxicity of
991 diverse neurodegenerative disease-linked proteins. *Dis Model Mech* 7, 1175-1184.
992 10.1242/dmm.016113.
- 993 37. Jackrel, M.E., and Shorter, J. (2014). Reversing deleterious protein aggregation with re-
994 engineered protein disaggregases. *Cell Cycle* 13, 1379-1383. 10.4161/cc.28709.
- 995 38. Jackrel, M.E., Tariq, A., Yee, K., Weitzman, R., and Shorter, J. (2014). Isolating
996 potentiated Hsp104 variants using yeast proteinopathy models. *J Vis Exp*, e52089.
997 10.3791/52089.

- 998 39. Ryan, J.J., Bao, A., Bell, B., Ling, C., and Jackrel, M.E. (2021). Drivers of Hsp104
999 potentiation revealed by scanning mutagenesis of the middle domain. *Protein Sci* 30,
1000 1667-1685. 10.1002/pro.4126.
- 1001 40. Ye, X., Lin, J., Mayne, L., Shorter, J., and Englander, S.W. (2020). Structural and kinetic
1002 basis for the regulation and potentiation of Hsp104 function. *Proc Natl Acad Sci U S A*
1003 117, 9384-9392. 10.1073/pnas.1921968117.
- 1004 41. Heuck, A., Schitter-Sollner, S., Suskiewicz, M.J., Kurzbauer, R., Kley, J., Schleiffer, A.,
1005 Rombaut, P., Herzog, F., and Clausen, T. (2016). Structural basis for the disaggregase
1006 activity and regulation of Hsp104. *Elife* 5. 10.7554/eLife.21516.
- 1007 42. Shorter, J., and Lindquist, S. (2008). Hsp104, Hsp70 and Hsp40 interplay regulates
1008 formation, growth and elimination of Sup35 prions. *EMBO J* 27, 2712-2724.
1009 10.1038/emboj.2008.194.
- 1010 43. Shorter, J. (2011). The mammalian disaggregase machinery: Hsp110 synergizes with
1011 Hsp70 and Hsp40 to catalyze protein disaggregation and reactivation in a cell-free
1012 system. *PLoS One* 6, e26319. 10.1371/journal.pone.0026319.
- 1013 44. Sweeny, E.A., and Shorter, J. (2008). Prion proteostasis: Hsp104 meets its supporting
1014 cast. *Prion* 2, 135-140. 10.4161/pri.2.4.7952.
- 1015 45. Dugaard, M., Rohde, M., and Jaattela, M. (2007). The heat shock protein 70 family:
1016 Highly homologous proteins with overlapping and distinct functions. *FEBS Lett* 581,
1017 3702-3710. 10.1016/j.febslet.2007.05.039.
- 1018 46. Ahmad, A., Bhattacharya, A., McDonald, R.A., Cordes, M., Ellington, B., Bertelsen, E.B.,
1019 and Zuideweg, E.R. (2011). Heat shock protein 70 kDa chaperone/DnaJ cochaperone
1020 complex employs an unusual dynamic interface. *Proc Natl Acad Sci U S A* 108, 18966-
1021 18971. 10.1073/pnas.1111220108.
- 1022 47. Cuellar, J., Perales-Calvo, J., Muga, A., Valpuesta, J.M., and Moro, F. (2013). Structural
1023 insights into the chaperone activity of the 40-kDa heat shock protein DnaJ: binding and
1024 remodeling of a native substrate. *J Biol Chem* 288, 15065-15074.
1025 10.1074/jbc.M112.430595.

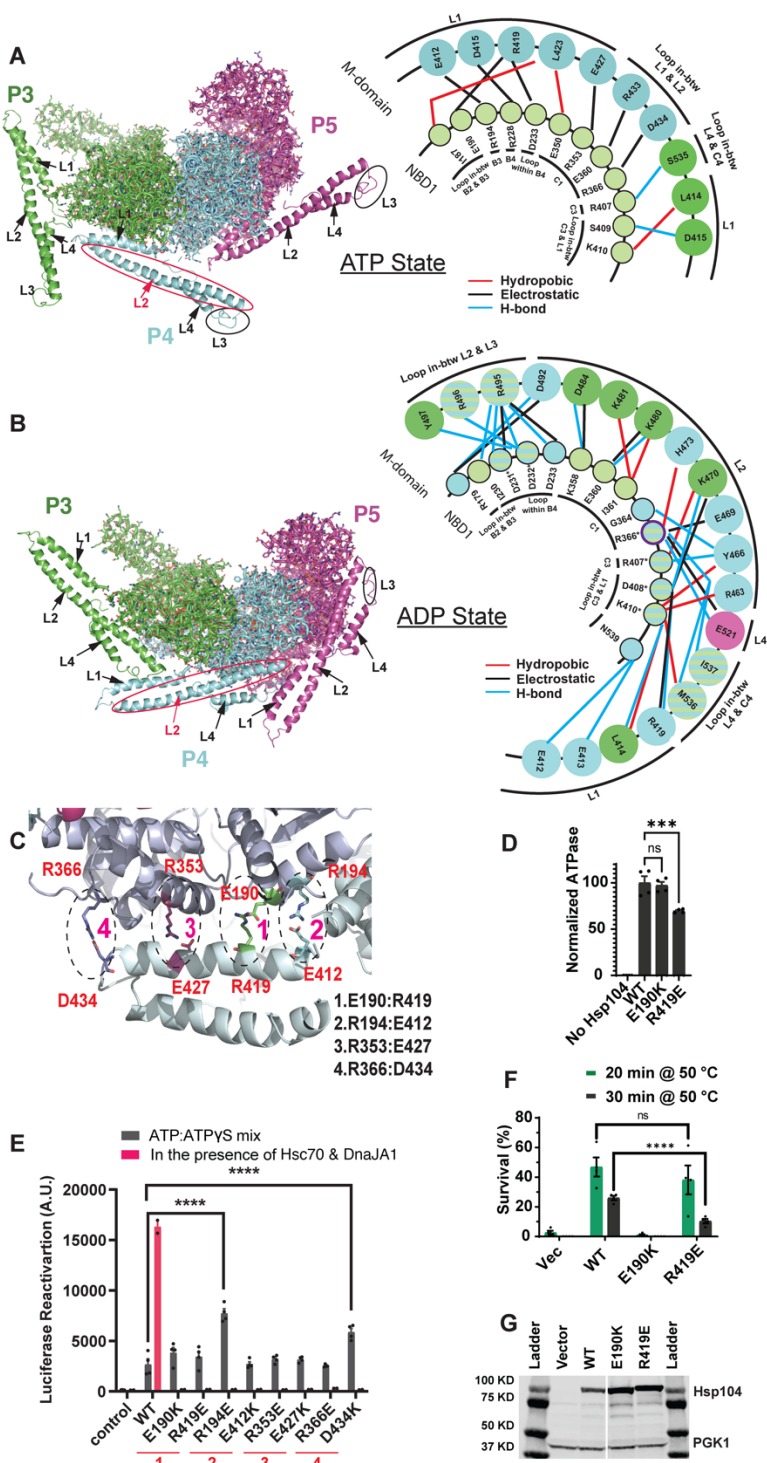
- 1026 48. Kampinga, H.H., and Craig, E.A. (2010). The HSP70 chaperone machinery: J proteins
1027 as drivers of functional specificity. *Nat Rev Mol Cell Biol* 11, 579-592. 10.1038/nrm2941.
- 1028 49. Lee, J., Kim, J.H., Biter, A.B., Sielaff, B., Lee, S., and Tsai, F.T. (2013). Heat shock
1029 protein (Hsp) 70 is an activator of the Hsp104 motor. *Proc Natl Acad Sci U S A* 110,
1030 8513-8518. 10.1073/pnas.1217988110.
- 1031 50. DeSantis, M.E., Sweeny, E.A., Snead, D., Leung, E.H., Go, M.S., Gupta, K., Wendler,
1032 P., and Shorter, J. (2014). Conserved distal loop residues in the Hsp104 and ClpB
1033 middle domain contact nucleotide-binding domain 2 and enable Hsp70-dependent
1034 protein disaggregation. *J Biol Chem* 289, 848-867. 10.1074/jbc.M113.520759.
- 1035 51. Sweeny, E.A., Tariq, A., Gurpinar, E., Go, M.S., Sochor, M.A., Kan, Z.Y., Mayne, L.,
1036 Englander, S.W., and Shorter, J. (2020). Structural and mechanistic insights into Hsp104
1037 function revealed by synchrotron X-ray footprinting. *J Biol Chem* 295, 1517-1538.
1038 10.1074/jbc.RA119.011577.
- 1039 52. Rosenzweig, R., Moradi, S., Zarrine-Afsar, A., Glover, J.R., and Kay, L.E. (2013).
1040 Unraveling the mechanism of protein disaggregation through a ClpB-DnaK interaction.
1041 *Science* 339, 1080-1083. 10.1126/science.1233066.
- 1042 53. Yin, Y., Feng, X., Yu, H., Fay, A., Kovach, A., Glickman, M.S., and Li, H. (2021).
1043 Structural basis for aggregate dissolution and refolding by the Mycobacterium
1044 tuberculosis ClpB-DnaK bi-chaperone system. *Cell Rep* 35, 109166.
1045 10.1016/j.celrep.2021.109166.
- 1046 54. Carroni, M., Kummer, E., Oguchi, Y., Wendler, P., Clare, D.K., Sinning, I., Kopp, J.,
1047 Mogk, A., Bukau, B., and Saibil, H.R. (2014). Head-to-tail interactions of the coiled-coil
1048 domains regulate ClpB activity and cooperation with Hsp70 in protein disaggregation.
1049 *Elife* 3, e02481. 10.7554/eLife.02481.
- 1050 55. Oguchi, Y., Kummer, E., Seyffer, F., Berynsky, M., Anstett, B., Zahn, R., Wade, R.C.,
1051 Mogk, A., and Bukau, B. (2012). A tightly regulated molecular toggle controls AAA+
1052 disaggregase. *Nat Struct Mol Biol* 19, 1338-1346. 10.1038/nsmb.2441.

- 1053 56. Sweeny, E.A., and Shorter, J. (2016). Mechanistic and Structural Insights into the Prion-
1054 Disaggregase Activity of Hsp104. *J Mol Biol* 428, 1870-1885.
1055 10.1016/j.jmb.2015.11.016.
- 1056 57. DeSantis, M.E., Leung, E.H., Sweeny, E.A., Jackrel, M.E., Cushman-Nick, M., Neuhaus-
1057 Follini, A., Vashist, S., Sochor, M.A., Knight, M.N., and Shorter, J. (2012). Operational
1058 plasticity enables hsp104 to disaggregate diverse amyloid and nonamyloid clients. *Cell*
1059 151, 778-793. 10.1016/j.cell.2012.09.038.
- 1060 58. Jackrel, M.E., Yee, K., Tariq, A., Chen, A.I., and Shorter, J. (2015). Disparate Mutations
1061 Confer Therapeutic Gain of Hsp104 Function. *ACS Chem Biol* 10, 2672-2679.
1062 10.1021/acscchembio.5b00765.
- 1063 59. Gates, S.N., Yokom, A.L., Lin, J., Jackrel, M.E., Rizo, A.N., Kendersky, N.M., Buell,
1064 C.E., Sweeny, E.A., Mack, K.L., Chuang, E., et al. (2017). Ratchet-like polypeptide
1065 translocation mechanism of the AAA+ disaggregase Hsp104. *Science* 357, 273-279.
1066 10.1126/science.aan1052.
- 1067 60. Rizo, A.N., Lin, J., Gates, S.N., Tse, E., Bart, S.M., Castellano, L.M., DiMaio, F., Shorter,
1068 J., and Southworth, D.R. (2019). Structural basis for substrate gripping and translocation
1069 by the ClpB AAA+ disaggregase. *Nat Commun* 10, 2393. 10.1038/s41467-019-10150-y.
- 1070 61. Yu, H., Lupoli, T.J., Kovach, A., Meng, X., Zhao, G., Nathan, C.F., and Li, H. (2018).
1071 ATP hydrolysis-coupled peptide translocation mechanism of *Mycobacterium tuberculosis*
1072 ClpB. *Proc Natl Acad Sci U S A* 115, E9560-e9569. 10.1073/pnas.1810648115.
- 1073 62. Sweeny, E.A., Jackrel, M.E., Go, M.S., Sochor, M.A., Razzo, B.M., DeSantis, M.E.,
1074 Gupta, K., and Shorter, J. (2015). The Hsp104 N-terminal domain enables disaggregase
1075 plasticity and potentiation. *Mol Cell* 57, 836-849. 10.1016/j.molcel.2014.12.021.
- 1076 63. Tariq, A., Lin, J., Jackrel, M.E., Hesketh, C.D., Carman, P.J., Mack, K.L., Weitzman, R.,
1077 Gambogi, C., Hernandez Murillo, O.A., Sweeny, E.A., et al. (2019). Mining Disaggregase
1078 Sequence Space to Safely Counter TDP-43, FUS, and alpha-Synuclein Proteotoxicity.
1079 *Cell Rep* 28, 2080-2095 e2086. 10.1016/j.celrep.2019.07.069.

- 1080 64. Tariq, A., Lin, J., Noll, M.M., Torrente, M.P., Mack, K.L., Murillo, O.H., Jackrel, M.E., and
1081 Shorter, J. (2018). Potentiating Hsp104 activity via phosphomimetic mutations in the
1082 middle domain. *FEMS Yeast Res* 18. 10.1093/femsyr/foy042.
- 1083 65. Torrente, M.P., Chuang, E., Noll, M.M., Jackrel, M.E., Go, M.S., and Shorter, J. (2016).
1084 Mechanistic Insights into Hsp104 Potentiation. *J Biol Chem* 291, 5101-5115.
1085 10.1074/jbc.M115.707976.
- 1086 66. Chamera, T., Klosowska, A., Janta, A., Wyszowski, H., Obuchowski, I., Gumowski, K.,
1087 and Liberek, K. (2019). Selective Hsp70-Dependent Docking of Hsp104 to Protein
1088 Aggregates Protects the Cell from the Toxicity of the Disaggregase. *J Mol Biol* 431,
1089 2180-2196. 10.1016/j.jmb.2019.04.014.
- 1090 67. DeSantis, M.E., and Shorter, J. (2012). The elusive middle domain of Hsp104 and ClpB:
1091 location and function. *Biochim Biophys Acta* 1823, 29-39.
1092 10.1016/j.bbamcr.2011.07.014.
- 1093 68. Cashikar, A.G., Schirmer, E.C., Hattendorf, D.A., Glover, J.R., Ramakrishnan, M.S.,
1094 Ware, D.M., and Lindquist, S.L. (2002). Defining a pathway of communication from the
1095 C-terminal peptide binding domain to the N-terminal ATPase domain in a AAA protein.
1096 *Mol Cell* 9, 751-760. 10.1016/s1097-2765(02)00499-9.
- 1097 69. Schirmer, E.C., Homann, O.R., Kowal, A.S., and Lindquist, S. (2004). Dominant gain-of-
1098 function mutations in Hsp104p reveal crucial roles for the middle region. *Mol Biol Cell* 15,
1099 2061-2072. 10.1091/mbc.e02-08-0502.
- 1100 70. Yokom, A.L., Gates, S.N., Jackrel, M.E., Mack, K.L., Su, M., Shorter, J., and Southworth,
1101 D.R. (2016). Spiral architecture of the Hsp104 disaggregase reveals the basis for
1102 polypeptide translocation. *Nat Struct Mol Biol* 23, 830-837. 10.1038/nsmb.3277.
- 1103 71. Doyle, S.M., Shorter, J., Zolkiewski, M., Hoskins, J.R., Lindquist, S., and Wickner, S.
1104 (2007). Asymmetric deceleration of ClpB or Hsp104 ATPase activity unleashes protein-
1105 remodeling activity. *Nat Struct Mol Biol* 14, 114-122. 10.1038/nsmb1198.
- 1106 72. Sanchez, Y., Parsell, D.A., Taulien, J., Vogel, J.L., Craig, E.A., and Lindquist, S. (1993).
1107 Genetic evidence for a functional relationship between Hsp104 and Hsp70. *J Bacteriol*
1108 175, 6484-6491. 10.1128/jb.175.20.6484-6491.1993.

- 1109 73. Moreau, K., Coen, M., Zhang, A.X., Pachel, F., Castaldi, M.P., Dahl, G., Boyd, H., Scott,
1110 C., and Newham, P. (2020). Proteolysis-targeting chimeras in drug development: A
1111 safety perspective. *Br J Pharmacol* 177, 1709-1718. 10.1111/bph.15014.
- 1112 74. Jiang, Y., Rossi, P., and Kalodimos, C.G. (2019). Structural basis for client recognition
1113 and activity of Hsp40 chaperones. *Science* 365, 1313-1319. 10.1126/science.aax1280.
- 1114 75. Caplan, A.J., Tsai, J., Casey, P.J., and Douglas, M.G. (1992). Farnesylation of YDJ1p is
1115 required for function at elevated growth temperatures in *Saccharomyces cerevisiae*. *J*
1116 *Biol Chem* 267, 18890-18895. 10.1016/S0021-9258(19)37044-9.
- 1117 76. Hildebrandt, E.R., Cheng, M., Zhao, P., Kim, J.H., Wells, L., and Schmidt, W.K. (2016).
1118 A shunt pathway limits the CaaX processing of Hsp40 Ydj1p and regulates Ydj1p-
1119 dependent phenotypes. *Elife* 5. 10.7554/eLife.15899.
- 1120 77. Wyszowski, H., Janta, A., Sztangierska, W., Obuchowski, I., Chamera, T., Kłosowska,
1121 A., and Liberek, K. (2021). Class-specific interactions between Sis1 J-domain protein
1122 and Hsp70 chaperone potentiate disaggregation of misfolded proteins. *Proc Natl Acad*
1123 *Sci U S A* 118. 10.1073/pnas.2108163118.
- 1124 78. Lum, R., Niggemann, M., and Glover, J.R. (2008). Peptide and protein binding in the
1125 axial channel of Hsp104. Insights into the mechanism of protein unfolding. *J Biol Chem*
1126 283, 30139-30150. 10.1074/jbc.M804849200.
- 1127 79. Lopez, K.E., Rizo, A.N., Tse, E., Lin, J., Scull, N.W., Thwin, A.C., Lucius, A.L., Shorter,
1128 J., and Southworth, D.R. (2020). Conformational plasticity of the ClpAP AAA+ protease
1129 couples protein unfolding and proteolysis. *Nat Struct Mol Biol* 27, 406-416.
1130 10.1038/s41594-020-0409-5.
- 1131 80. Fare, C.M., Rhine, K., Lam, A., Myong, S., and Shorter, J. (2023). A minimal construct of
1132 nuclear-import receptor Karyopherin-beta2 defines the regions critical for chaperone and
1133 disaggregation activity. *J Biol Chem* 299, 102806. 10.1016/j.jbc.2022.102806.
- 1134 81. Rohner, E., Yang, R., Foo, K.S., Goedel, A., and Chien, K.R. (2022). Unlocking the
1135 promise of mRNA therapeutics. *Nat Biotechnol* 40, 1586-1600. 10.1038/s41587-022-
1136 01491-z.

- 1137 82. Han, E.L., Padilla, M.S., Palanki, R., Kim, D., Mrksich, K., Li, J.J., Tang, S., Yoon, I.C.,
1138 and Mitchell, M.J. (2024). Predictive High-Throughput Platform for Dual Screening of
1139 mRNA Lipid Nanoparticle Blood-Brain Barrier Transfection and Crossing. *Nano Lett.*
1140 10.1021/acs.nanolett.3c03509.
- 1141 83. Cupo, R.R., and Shorter, J. (2020). Expression and Purification of Recombinant Skd3
1142 (Human ClpB) Protein and Tobacco Etch Virus (TEV) Protease from *Escherichia coli*.
1143 *Bio Protoc* 10, e3858. 10.21769/BioProtoc.3858.
- 1144 84. Michalska, K., Zhang, K., March, Z.M., Hatzos-Skintges, C., Pintilie, G., Bigelow, L.,
1145 Castellano, L.M., Miles, L.J., Jackrel, M.E., Chuang, E., et al. (2019). Structure of
1146 *Calcarisporiella thermophila* Hsp104 Disaggregase that Antagonizes Diverse Proteotoxic
1147 Misfolding Events. *Structure* 27, 449-463 e447. 10.1016/j.str.2018.11.001.
- 1148 85. Rueden, C.T., Schindelin, J., Hiner, M.C., DeZonia, B.E., Walter, A.E., Arena, E.T., and
1149 Eliceiri, K.W. (2017). ImageJ2: ImageJ for the next generation of scientific image data.
1150 *BMC Bioinformatics* 18, 529. 10.1186/s12859-017-1934-z.
- 1151 86. Braig, K., Otwinowski, Z., Hegde, R., Boisvert, D.C., Joachimiak, A., Horwich, A.L., and
1152 Sigler, P.B. (1994). The crystal structure of the bacterial chaperonin GroEL at 2.8 Å.
1153 *Nature* 371, 578-586. 10.1038/371578a0.
- 1154 87. Gietz, R.D., and Schiestl, R.H. (2007). High-efficiency yeast transformation using the
1155 LiAc/SS carrier DNA/PEG method. *Nat Protoc* 2, 31-34. 10.1038/nprot.2007.13.
- 1156
- 1157



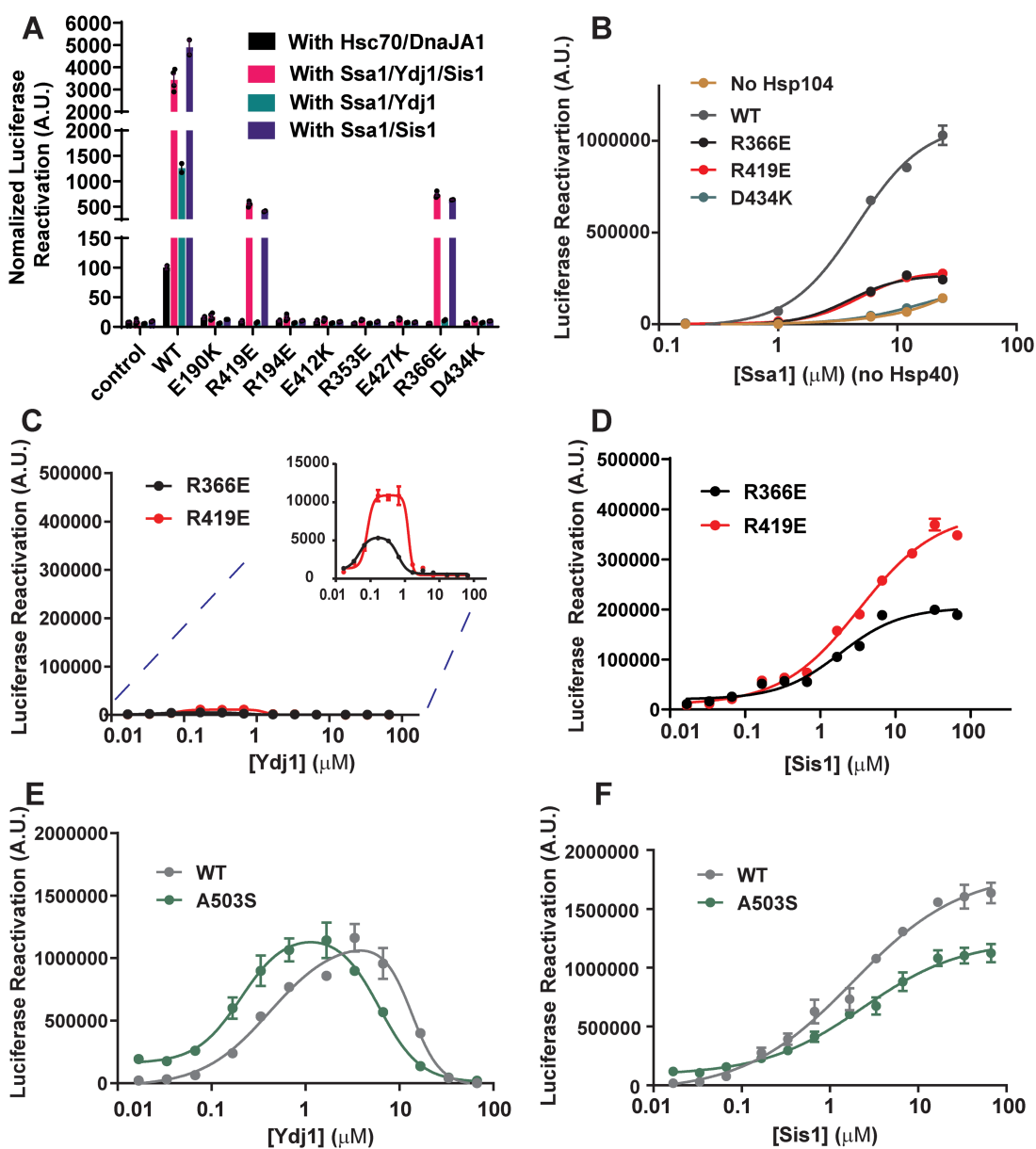
1158

1159 **Figure 1. The MD changes orientation as Hsp104 hexamers switch from ATP-bound to**
 1160 **ADP-bound states, which alter NBD1:MD interactions. (A, B) Left, three out of six protomers**
 1161 **(P3 in green, P4 in blue, and P5 in magenta) are shown for the ATP state (A) or ADP state (B).**
 1162 **NBD1 is shown in ribbon and MD is shown in cartoon. The four MD helices (L1, L2, L3, and L4)**
 1163 **are indicated by arrows. However, MD helix L3 appears to be a loop in these structures. Right,**
 1164 **the NBD1:MD interactions for protomers P3 (Green) and P4 (Blue) were analyzed using**

1165 Discovery Studio Visualizer with a 4Å cut off distance for the ATP-bound state (AMP-PNP, 5KNE)
1166 (A) or the ADP-bound state (5VY8) (B). Hydrophobic, electrostatic (salt-bridge), and hydrogen
1167 bond interactions are indicated in red, black, and blue lines, respectively. For the ATP-bound state
1168 (A), NBD1:MD interactions were observed between the NBD1 of P3 (green circles) and MD of P4
1169 (blue circles). For the ADP-bound state (B), we show NBD1:MD interactions within P3 (green
1170 circles) or within P4 (blue circles) and a unique interaction between R366 and E521 within P5
1171 (purple) for clarity. Intrasubunit NBD1:MD interactions conserved in P3 and P4 are shown in
1172 circles with blue and green stripes. Residues involved in intrasubunit NBD1:MD interactions for
1173 P3, P4 or P5 are shown in circles with blue and green stripes with an '*'. **(C)** NBD1:MD helix L1
1174 interactions with NBD1 in the ATP state. Four major salt-bridge interactions: 1. E190:R419, 2.
1175 R194:E412, 3. R353:E427 and 4. R366:D434, are identified on the inter-subunit NBD1:MD
1176 interface in the presence of AMP-PNP. E190, R194, R353, and R366 are in NBD1 of subunit P3,
1177 and R419, E412, E427 and D434 are in MD helix L1 of P4. **(D)** ATPase activity of Hsp104,
1178 Hsp104^{E190K}, and Hsp104^{R419E} (0.25μM) in the presence of 1mM ATP at 25°C. Bars represent
1179 means±SEM (n=4); each replicate is shown as a dot. Ordinary one-way ANOVA Dunnett's test
1180 was performed to compare the ATPase activity of Hsp104 to Hsp104^{E190K} or Hsp104^{R419E}. ns=not
1181 significant; ***p=0.0005. **(E)** Hsp104 variants (1μM, monomer) in the presence of ATP:ATPyS
1182 (2.5mM:2.5 mM; black bars) or with Hsc70 (0.167μM) and DnaJA1 (0.167μM; pink bars) were
1183 incubated with 100nM (monomeric concentration) chemical-denatured luciferase aggregates for
1184 90min at 25°C. Buffer serves as the negative control. Bars represent means±SEM (n=4); each
1185 replicate is shown as a dot. ****P≤0.0001. **(F)** Survival (%) of *Δhsp104* yeast transformed with
1186 empty vector (pRS313HSE), Hsp104, Hsp104^{E190K}, or Hsp104^{R419E} after 0, 20, or 30min heat
1187 shock at 50°C following a pretreatment at 37°C for 30min. Bars represent means±SEM (n=4);
1188 each replicate is shown as a dot. ns=not significant; ****P≤0.0001. **(G)** *Δhsp104* yeast from (F)
1189 were incubated at 37°C for 30 min to induce Hsp104 expression. Yeast were then lysed and
1190 processed for Western blot. 3-Phosphoglycerate kinase 1 (PGK1) serves as a loading control.

1191 See also Figure S1.

1192



1193

1194 **Figure 2. Specific perturbation of ATP-specific NBD1:MD helix L1 contacts yields Hsp104**

1195 **variants that collaborate selectively with class B Hsp40s. (A)** Luciferase disaggregation and

1196 reactivation activity of the indicated Hsp104 variants (1 μ M, monomeric) in the presence of Hsc70

1197 (0.167 μ M) and DnaJA1 (0.167 μ M; black), Ssa1 (0.167 μ M), Ydj1 (0.083 μ M), and Sis1 (0.083 μ M;

1198 pink), Ssa1 (0.167 μ M) and Ydj1 (0.167 μ M; green), or Ssa1 (0.167 μ M) and Sis1 (0.167 μ M;

1199 purple). Bars represent means \pm SEM (n=2-4), each replicate is shown as a dot. **(B)** Luciferase

1200 disaggregation and reactivation activity of Hsp104 (grey dots), Hsp104^{R366E} (black dots),

1201 Hsp104^{R419E} (red dots), or Hsp104^{D434K} (teal dots; 1 μ M, monomeric) in the presence of various

1202 Ssa1 (Hsp70) concentrations in the absence of Hsp40. Curves were fit for absolute EC₅₀ (see

1203 STAR Methods and Table S1). Values represent means \pm SEM (n=2). **(C, D)** Luciferase

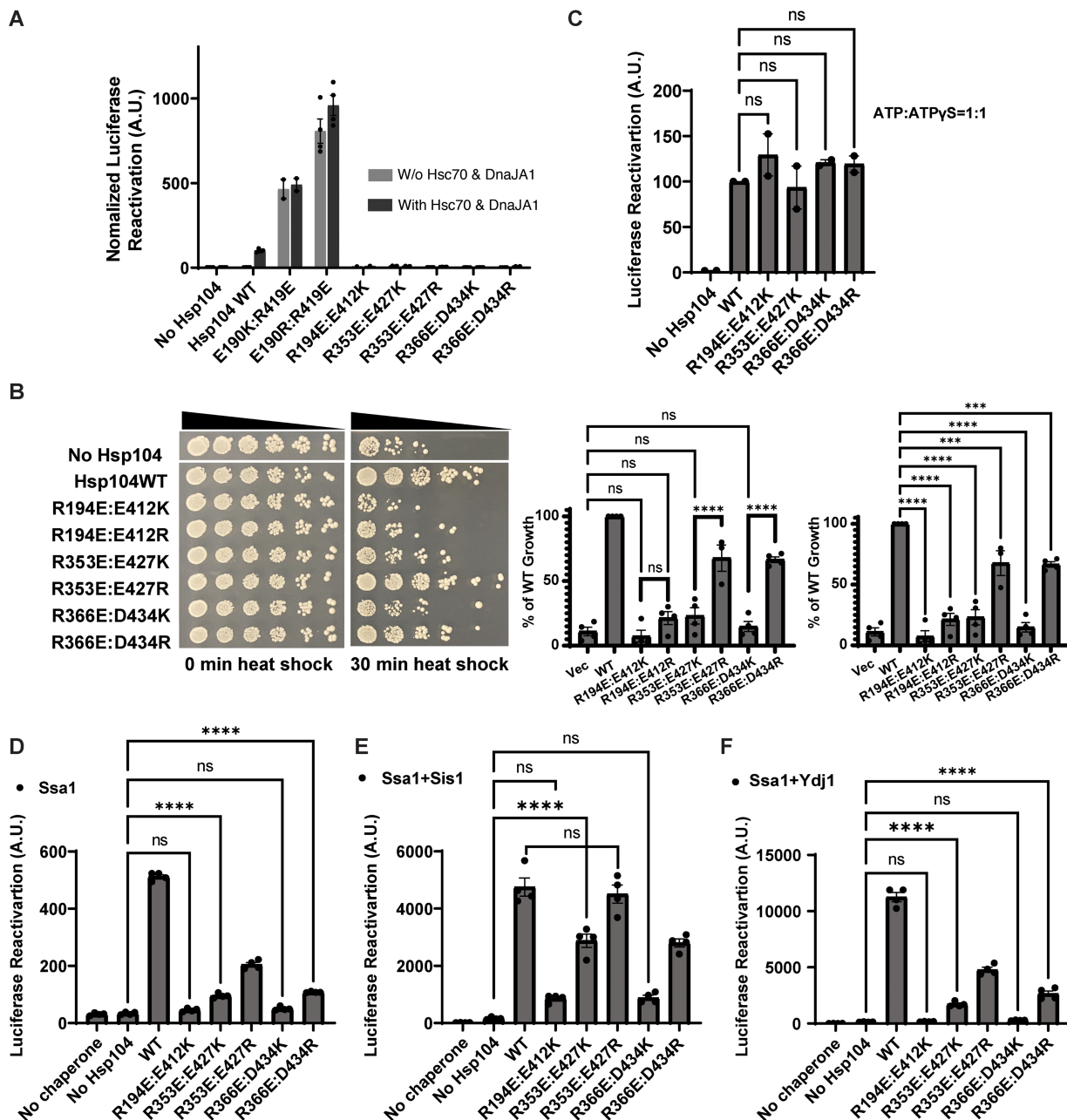
1204 disaggregation and reactivation activity of Hsp104^{R366E} (1 μ M monomeric) plus Ssa1 (0.167 μ M;

1205 black) or Hsp104^{R419E} (1 μ M monomeric) plus Ssa1 (0.167 μ M; red) as a function of Ydj1 (C) or

1206 Sis1 (D) concentration. Curves were fit for IC₅₀ of Ydj1 and EC₅₀ of Ydj1 or Sis1 (see STAR
1207 Methods and Table S1). Values represent means±SEM (n=2). **(E, F)** Luciferase disaggregation
1208 and reactivation activity of Hsp104 (1μM, monomeric) plus Ssa1 (0.167μM; grey) or Hsp104^{A503S}
1209 (1μM, monomeric) plus Ssa1 (0.167μM; green) as a function of Ydj1 (E) or Sis1 (F) concentration.
1210 Curves were fit for IC₅₀ of Ydj1 and EC₅₀ of Ydj1 or Sis1 (see STAR Methods and Table S1).
1211 Values represent means±SEM (n=2).

1212 See also Figure S1, S2 and Table S1.

1213



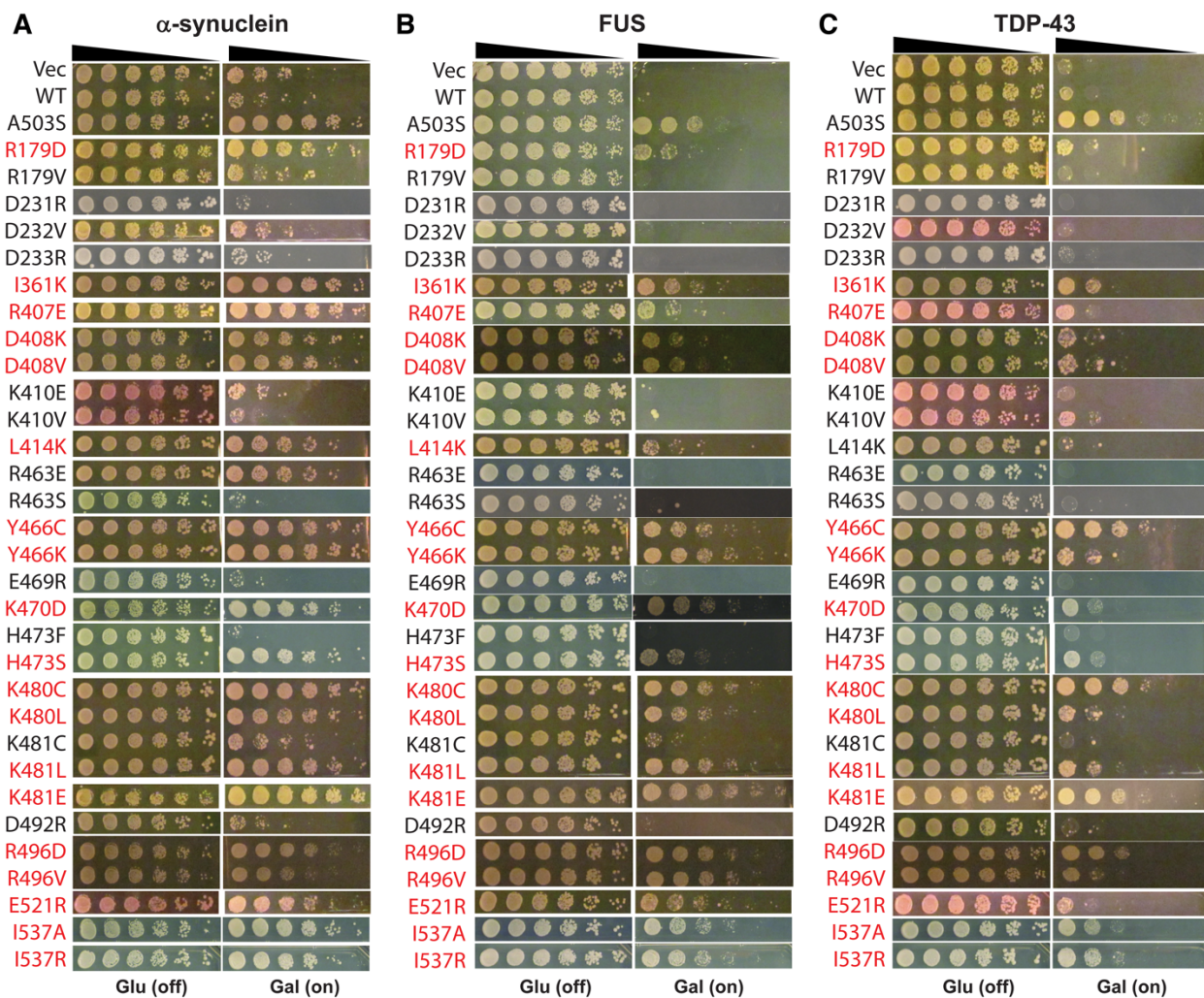
1214

1215 **Figure 3. Rewiring the ATP-specific interprotomer NBD1:MD helix L1 interaction alters**
 1216 **Hsp104 collaboration with Hsp70 and Hsp40. (A)** Luciferase disaggregation and reactivation
 1217 activity of the indicated Hsp104 variants (1 μ M, monomeric) in the absence (grey bars) or presence
 1218 (black bars) of Hsc70 (0.167 μ M) and DnaJA1 (0.167 μ M). Bars represent means \pm SEM (N=2-4);
 1219 each replicate is shown as a dot. One-way ANOVA Dunnett's test was performed to compare
 1220 Hsp104 to Hsp104 variants at a 95% confidence interval (CI). The luciferase disaggregation and
 1221 reactivation activity of all tested Hsp104 variants is significantly different from Hsp104 with
 1222 ****P \leq 0.0001 (statistics are omitted for clarity). **(B)** Left, spotting assay to evaluate the survival of
 1223 Δ *hsp104* yeast transformed with empty vector (no Hsp104) or the indicated Hsp104 variants
 1224 (WT=wild type) after a 30min pretreatment at 37 $^{\circ}$ C followed by a 30min heat shock at 50 $^{\circ}$ C.

1225 *Δhsp104* yeast that were not heat shocked are shown on the left as a control. Right panels, yeast
1226 survival (% of wild-type Hsp104) was quantified. Bars represent means±SEM (n=4), and each
1227 replicate is shown as a dot. One-way ANOVA Dunnett's tests were performed to compare Hsp104
1228 variants to no Hsp104 control (middle panel) or WT (right panel) at 95% CI. ns=not significant;
1229 ***P≤0.001 ****P≤0.0001. One-way ANOVA Tukey tests were performed to make pairwise
1230 comparisons between specific Hsp104 variants as indicated (middle panel) ****P≤0.0001. **(C)**
1231 Luciferase disaggregation and reactivation activity of the indicated Hsp104 variants (1μM,
1232 monomeric) in the presence of ATP:ATPγS (2.5mM:2.5mM) and the absence of Hsp70 and
1233 Hsp40. Bars represent means±SEM (n=2), and each replicate is shown as a dot. One-way
1234 ANOVA Dunnett's test was performed to compare Hsp104 variants to Hsp104 at 95% CI. ns=not
1235 significant. **(D)** Luciferase disaggregation and reactivation activity of the indicated Hsp104
1236 variants (1μM monomeric) in the presence of Ssa1 (0.167μM) and absence of Hsp40. Bars
1237 represent means±SEM (n=4); each replicate is shown as a dot. One-way ANOVA Dunnett's test
1238 was performed to compare Hsp104 variants to WT Hsp104 at 95% CI. All variants have
1239 significantly reduced activity to work with Ssa1 compared to WT Hsp104 with a P≤0.0001
1240 (statistics are omitted for clarity). Alternatively, one-way ANOVA Dunnett's test was performed to
1241 compare Hsp104 variants to no Hsp104. ns=not significant; ****P≤0.0001. **(E)** Luciferase
1242 disaggregation and reactivation activity of the indicated Hsp104 variants (1μM, monomeric) in the
1243 presence Ssa1 (0.167μM) and Sis1 (0,167μM). Bars represent means±SEM (n=4), and each
1244 replicate is shown as a dot. One-way ANOVA Dunnett's test was performed to compare Hsp104
1245 variants to WT Hsp104 at 95% CI. ns=not significant. All other variants have reduced activity with
1246 a P≤0.0001 (statistics are omitted for clarity). Alternatively, one-way ANOVA Dunnett's test was
1247 performed to compare Hsp104 variants to no Hsp104. Ns=not significant, ****P≤0.0001. **(F)**
1248 Luciferase disaggregation and reactivation activity of the indicated Hsp104 variants (1μM,
1249 monomeric) in the presence of Ssa1 (0.167μM) and Ydj1 (0.167μM). Bars represent means±SEM
1250 (n=4); each replicate is shown as a dot. One-way ANOVA Dunnett's test was performed to
1251 compare Hsp104 variants to WT Hsp104 at 95% CI. All Hsp104 variants have reduced activity
1252 with a ****P≤0.0001 (statistics are omitted for clarity). Alternatively, one-way ANOVA Dunnett's
1253 test was performed to compare Hsp104 variants to no Hsp104. ns=not significant, ****P≤0.0001.

1254 See also Figure S3.

1255



1256

1257 **Figure 4. Perturbing the intraprotomer NBD1:MD contacts of the ADP state frequently**
 1258 **potentiates Hsp104 activity. (A-C)** $\Delta hsp104$ yeast integrated with α -synuclein-YFP (A) FUS (B),
 1259 or TDP-43 (C) on a galactose-inducible promoter were transformed with the indicated Hsp104
 1260 variants that perturb the intraprotomer NBD1:MD contacts of the ADP state. Empty vector and
 1261 WT Hsp104 are negative controls, and Hsp104^{A503S} is a positive control. Yeast were spotted onto
 1262 glucose (induction is off) and galactose (induction is on) media in a five-fold serial dilution.
 1263 Potentiated Hsp104 variants are highlighted in red. Western blots were performed to evaluate
 1264 Hsp104 expression, see Figure S4.

1265 See also Figure S4 and Table S2.

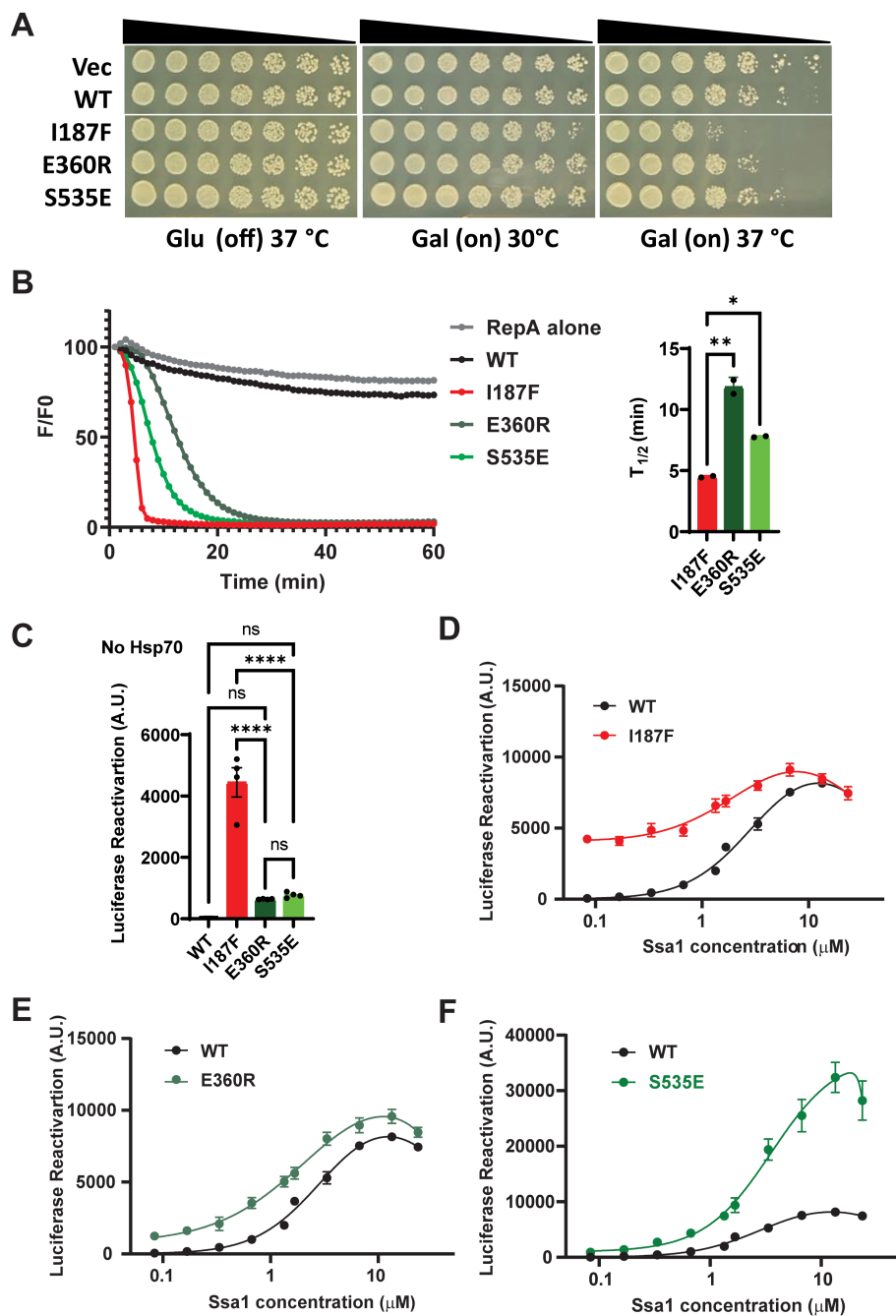


Figure 5. Restricting Hsp104 activity in the absence of Hsp70 reduces off-target toxicity of potentiated Hsp104 variants. (A) $\Delta hsp104$ yeast were transformed with the indicated galactose-inducible Hsp104 variants or an empty vector or Hsp104 control. Yeast were spotted onto glucose (induction off) and galactose (induction on) media in a five-fold serial dilution. Yeast were incubated on a glucose plate 37°C (left) or on a galactose plate at 30°C (middle) or 37°C (right). Note that Hsp104^{I187F} is more toxic than Hsp104^{E360R} or Hsp104^{S535E}. Hsp104^{E360R} and Hsp104^{S535E} are similar to Hsp104 at 37°C on galactose. **(B)** RepA₁₋₁₅-GFP (0.7μM) unfolding activity of the indicated Hsp104 variant (6μM, monomeric) in the presence of ATP (4mM) and GroEL_{trap} (2.5μM). RepA₁₋₁₅-GFP unfolding (%) was assessed by the RepA₁₋₁₅-GFP fluorescence signal at the indicated time (F), divided by the RepA₁₋₁₅-GFP fluorescence signal at

time 0 (F0). Left, kinetics of RepA₁₋₁₅-GFP unfolding. Results from a representative experiment are shown. Right, the half time of RepA₁₋₁₅-GFP unfolding for each Hsp104 variant. Bars represent means±SEM (N=2), each replicate is shown as a dot. One-way ANOVA Tukey test was performed to compare the half-time of one Hsp104 variant to every other one at 95% CI. *P=0.0117, **P=0.0012 for I187F vs. E360R, **P=0.0063 for E360R vs. S535E. **(C)** Luciferase disaggregation and reactivation by Hsp104, Hsp104^{I187F}, Hsp104^{E360R}, or Hsp104^{S535E} in the absence of Hsp70 and Hsp40. The indicated Hsp104 variant (1μM, monomeric) was incubated with chemically denatured luciferase aggregates (100 nM monomer concentration) for 90 min. Bars represent means±SEM (N=4), each replicate is shown as a dot. One-way ANOVA Tukey test was performed to compare the level of reactivated luciferase aggregates by Hsp104 variants at 95% CI. **** P≤0.0001. **(D-F)** Luciferase disaggregation and reactivation by Hsp104 (black curve), Hsp104^{I187F} (D, red curve), Hsp104^{E360R} (E, green curve) and Hsp104^{S535E} (F, green curve) as a function of Ssa1 concentration as indicated on the x-axis (log scale). The indicated Hsp104 variant (1μM, monomeric) in the presence of various Ssa1 concentrations was incubated with chemically denatured luciferase aggregates (100 nM monomer concentration). Values represent means±SEM (N=2). A bell-shaped dose-dependent curve is used to fit the data; see STAR Methods.

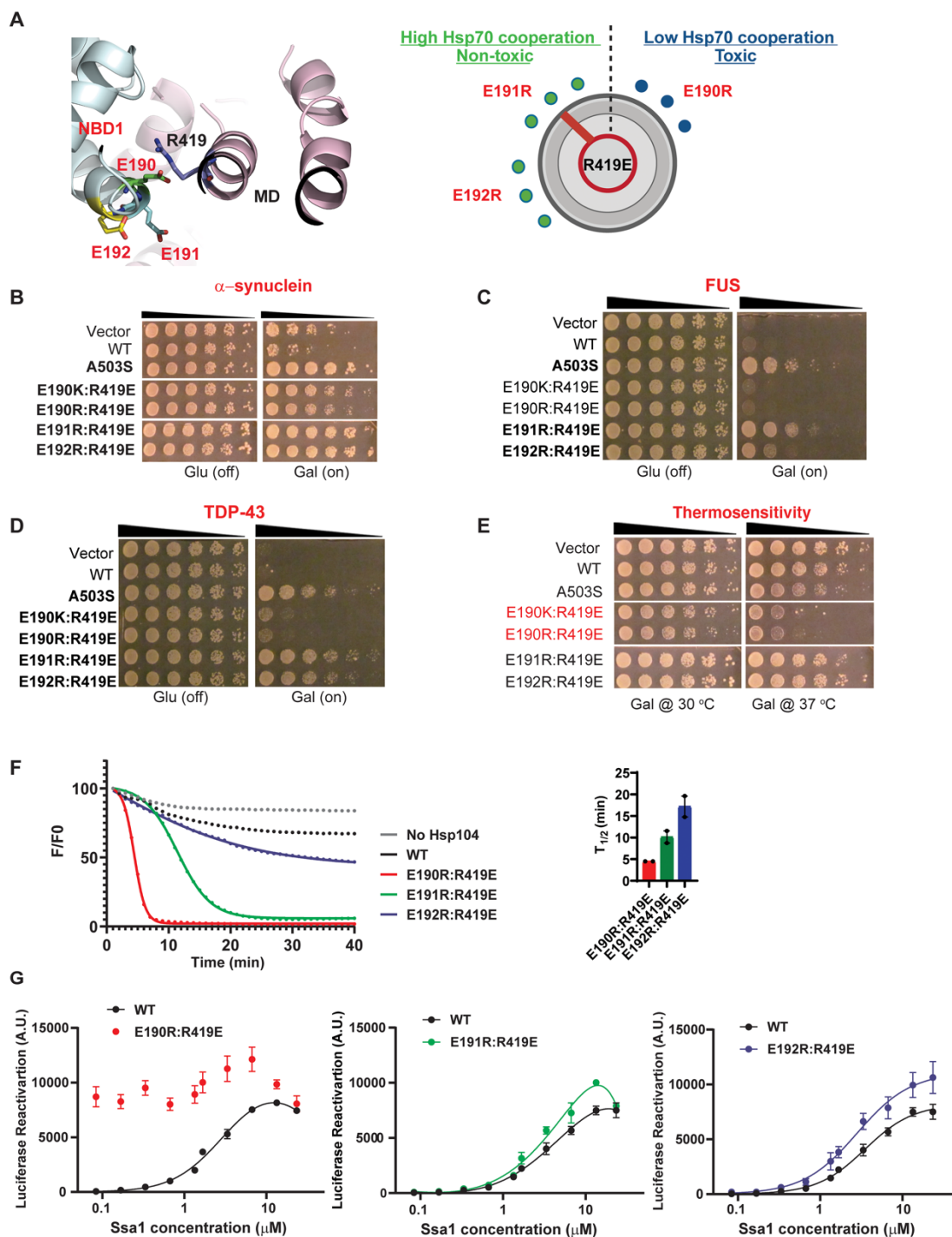


Figure 6. Rational design of potentiated Hsp104 variants with minimized off-target toxicity. (A) NBD1 (blue) residues E190, E191, and E192 (in red) form a rheostat-like interaction with R419 (black) in the MD (colored in pink) of the adjacent subunit. Hsp104 variants are designed to alter these interactions like a rheostat (right panel) to tune Hsp104-Hsp70 interaction to a suitable level of potentiated activity without off-target toxicity. (B-D) Spotting assay testing the ability of Hsp104 variants to mitigate α -synuclein (B), FUS (C), and TDP-43 (D) toxicity in yeast. $\Delta hsp104$ yeast integrated with α -synuclein (B), FUS (C), and TDP-43 (D) on a galactose-inducible promoter were transformed with Hsp104 variants or an empty

vector, WT Hsp104 or Hsp104^{A503S} controls. Yeast were spotted onto glucose (induction off) and galactose (induction on) media in a five-fold serial dilution. The variants that have potentiated activity to mitigate disease protein toxicity in yeast are highlighted in bold. **(E)** The toxicity of designed Hsp104 variants in yeast were evaluated at 37°C. *Δhsp104* yeast were transformed with galactose-inducible Hsp104 variants or an empty vector, WT Hsp104 or Hsp104^{A503S} controls. The yeast were spotted onto glucose (induction off) and galactose (induction on) media in a five-fold serial dilution. Yeast were incubated at 30°C (left) or 37°C (right) on galactose plates. The toxic variants are highlighted in red. **(F)** RepA₁₋₁₅-GFP (0.7μM) unfolding kinetics by Hsp104^{E190R:R419E}, Hsp104^{E191R:R419E}, or Hsp104^{E192R:R419E} (6μM, monomeric concentration) is measured in the presence of a GroEL_{trap} (2.5μM). RepA₁₋₁₅-GFP unfolding (%) was assessed by the RepA₁₋₁₅-GFP fluorescence signal at the indicated time (F), divided by the RepA₁₋₁₅-GFP fluorescence signal at time 0 (F0). Results from a representative experiment are shown. The half-time of RepA₁₋₁₅-GFP unfolding for each Hsp104 is shown on the right. Bars represent means±SEM (N=2), each replicate is shown as a dot. **(G)** Luciferase disaggregation and reactivation by Hsp104 (black curve), Hsp104^{E190R:R419E} (red curve, left), Hsp104^{E191R:R419E} (red curve, middle) and Hsp104^{E192R:R419E} (red curve, right) as a function of Ssa1 concentration. The indicated Hsp104 variant (1μM, monomeric) in the presence of various Ssa1 concentrations as indicated on the x-axis (log scale) was incubated with chemically denatured luciferase aggregates (100nM monomer concentration) for 90 min. Values represent means±SEM (N=2). A bell-shaped dose-dependent curve is used to fit the data, see STAR Methods.

See also Figure S5.

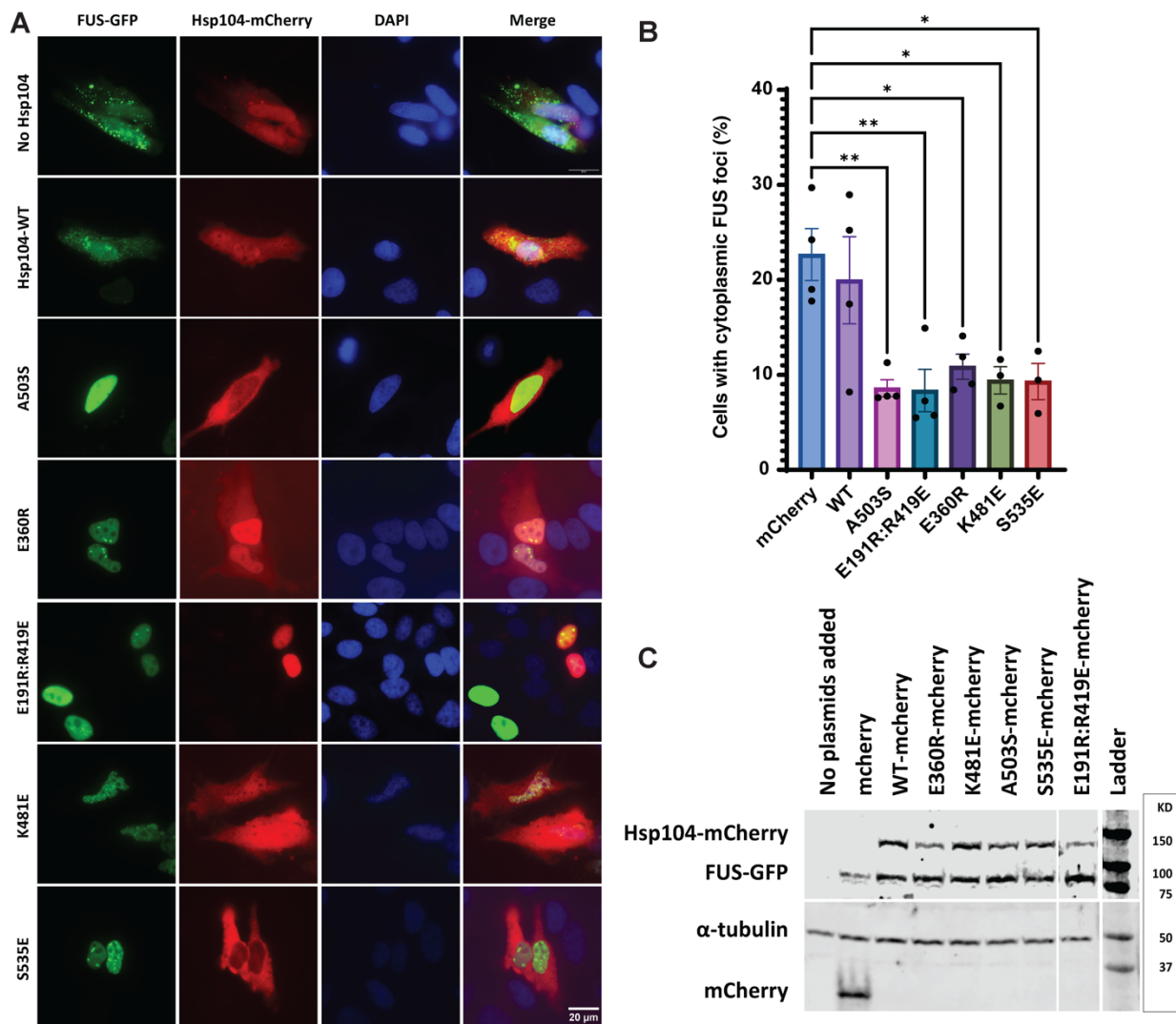


Figure 7. Potentiated Hsp104 variants suppress FUS proteinopathy in human cells. (A) After 24h, HeLa cells transfected with GFP-FUS (Green) and mCherry, or the indicated Hsp104 variant-mCherry (Red) were fixed and imaged. DAPI is used to stain the nucleus. Representative images are shown. Scale bar, 20 μ m. **(B)** Quantification of the percentage of cells with cytoplasmic FUS foci. 500 to 800 cells were counted over four separate trials for each Hsp104 variant and mCherry control; data points represent independent transfections. Bars represent means \pm SEM (N=4). One-way ANOVA with correction for multiple comparisons by Dunnett's test was performed at 95% CI. **P \leq 0.01; *P \leq 0.05. **(C)** Western blot of lysates of HeLa cells transfected with GFP-FUS and either mCherry alone or mCherry-tagged Hsp104. Probing with anti-GFP and anti-mCherry shows FUS-GFP and Hsp104-mCherry expression levels, respectively. α -tubulin is used as a loading control.

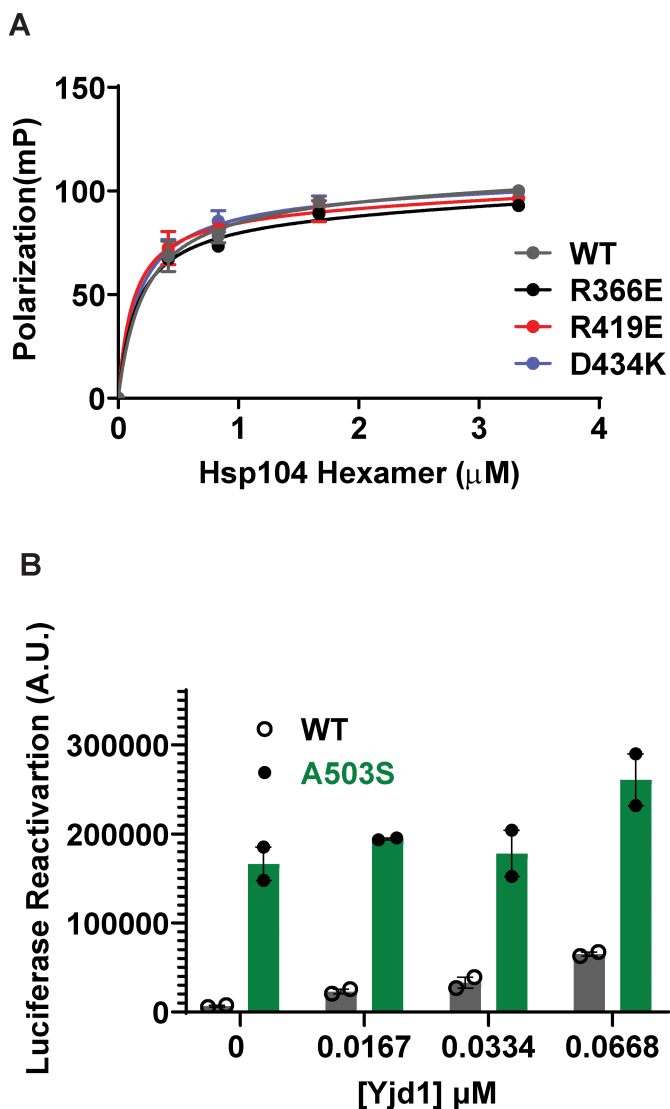


Figure S1. Hsp104 variants bind a model, disordered substrate, β -casein, with the same affinity as Hsp104 (A) FITC-casein (30nM) was incubated with the indicated concentration of Hsp104 (x-axis) in the presence of ATP γ S (2mM). Binding was assessed by fluorescence polarization. Values represent means \pm SEM (N=2). The data were fitted using a one-site binding curve in Graphpad, and the apparent K_D of the Hsp104 variants tested are similar to WT Hsp104 ($0.2\pm 0.1\mu\text{M}$). **(B)** Bar graph of the data presented in Figure 2E for luciferase disaggregation and reactivation by Hsp104 or Hsp104^{A503S} (1 μM , monomeric), plus Ssa1 (0.167 μM) and the three lowest Ydj1 concentrations or in the absence of Ydj1. Bars represent means \pm SEM (N=2); each data point represents an independent replicate.

Related to Figure 1 and 2.

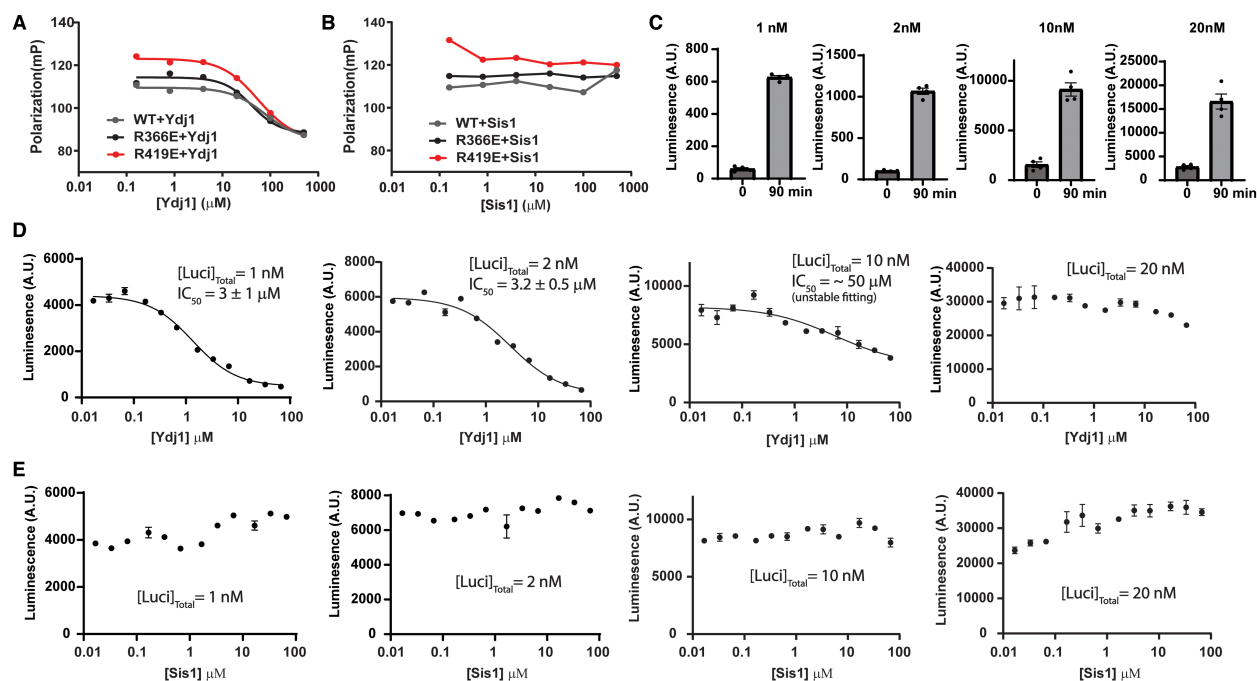


Figure S2. Ydj1 but not Sis1 can dissociate substrate from Hsp104 and inhibit the spontaneous refolding of unfolded luciferase. (A, B) Fluorescence polarization experiments measuring substrate binding competition between Hsp104 and Hsp40. Hsp104 (5 μM hexameric) and the model substrate, FITC-casein (30 nM), were incubated with ATP γS (2mM) for 30min. The complex was then titrated with Ydj1 (A) or Sis1(B) at the indicated concentrations (x-axis, log scale) in the presence of ATP γS (2mM). Fluorescence polarization of FITC-casein (y-axis) was measured. Results from a representative experiment are shown. (C) Spontaneous refolding of soluble unfolded luciferase in buffer was measured at time of unfolding (0 min) and after 90 min. Luciferase (10 μM) in 6M urea was incubated on ice for 5min and then diluted into solutions to a final concentration of 1, 2, 10 or 20nM as indicated in the figure. Luciferase activity was measured right after the unfolding reaction or after 90min in buffer. Bars represent means \pm SEM (N=4), each replicate is shown as a dot. (D, E) Luciferase (10 μM) in 6M urea was incubated on ice for 5 min and then diluted into solutions containing various concentrations of Ydj1 (panel D x-axis, log scale) or Sis1 (panel E x-axis, log scale) to a final concentration of 1, 2, 10 or 20nM as indicated. Luciferase activity was measured after 90min. Values represent means \pm SEM (N=2). The IC_{50} of Ydj1 inhibition was determined using the dose-dependent fitting model for absolute IC_{50} .

Related to Figure 2 and Table S1.

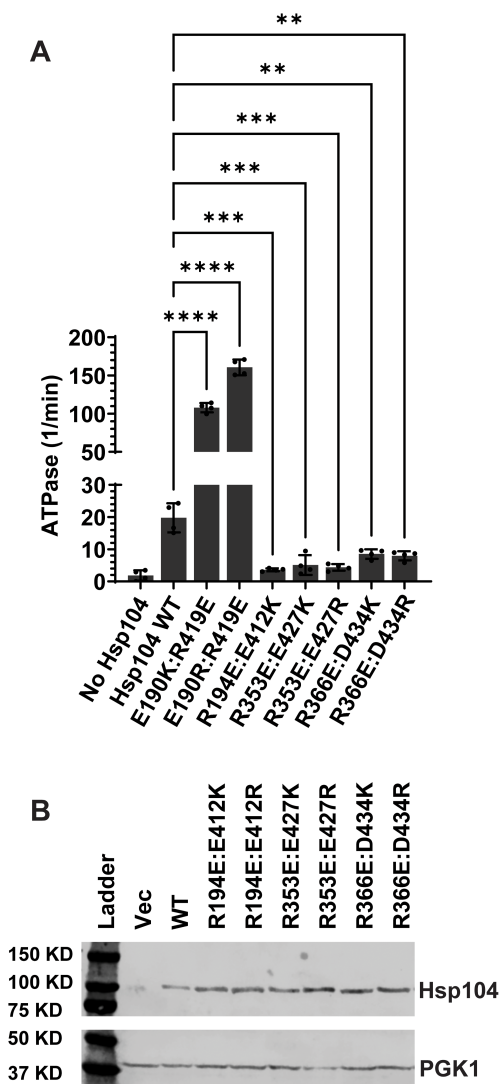


Figure S3. Rebuilding of the NBD1:MD salt bridges alters the ATPase activity of Hsp104.

(A) ATPase activity of the indicated Hsp104 variants (0.25 μ M, monomeric) in ATP (1mM) after 5min at 25°C. Bars represent means \pm SEM (N=4), individual replicates are shown as dots. Dunnett's multiple comparisons were performed to compare the ATP hydrolysis rate of NBD1-MD variants to WT. **** P \leq 0.0001, ***P \leq 0.001, **P \leq 0.01. (B) Western blots to evaluate Hsp104 expression level of yeast in the thermotolerance assay (Figure 3B). Hsp104 variants were expressed for 30min at 37°C in Δ *hsp104* yeast. Yeast were then lysed, and the lysates were processed for Western blot. PGK1 serves as a loading control.

Related to Figure 3.

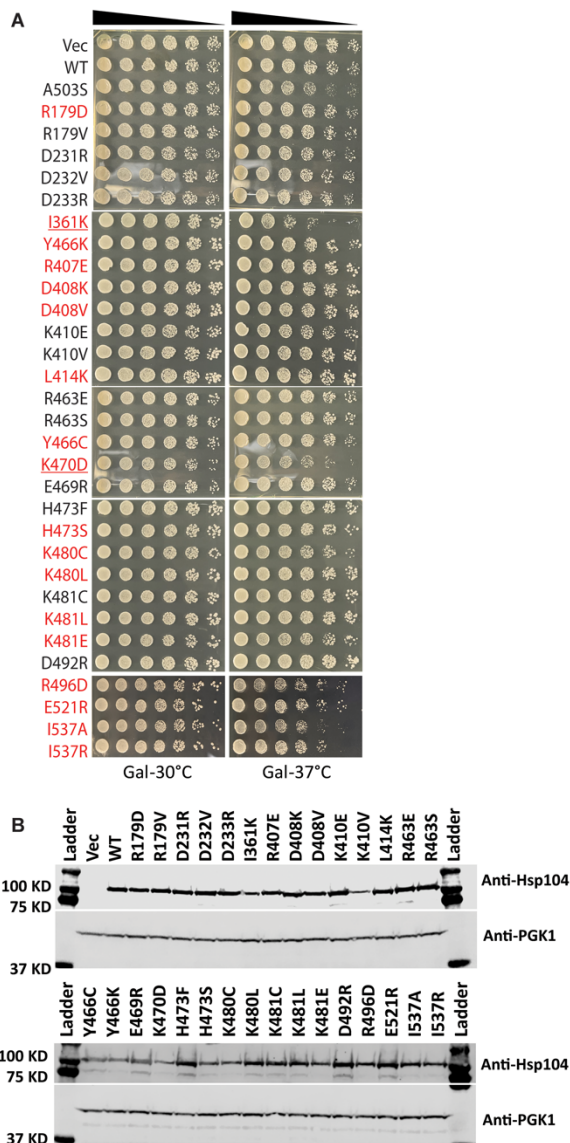


Figure S4. Hsp104 variant off-target toxicity and expression level in yeast. (A) The off-target toxicity of Hsp104 variants that perturb the intraprotomer NBD1:MD contacts of the ADP state is evaluated at 37°C using yeast spotting assay. $\Delta hsp104$ yeast were transformed with galactose-inducible Hsp104 variants or an empty vector, WT Hs104 or Hsp104^{A503S} serve as controls. The yeast were spotted onto galactose (induction on) media in a five-fold serial dilution and incubated at 30°C (left) or 37°C (right). The potentiated variants revealed in Figure 4 are highlighted in red, and the toxic variants are underlined. (B) Western blots were performed to evaluate Hsp104 expression. $\Delta hsp104$ yeast from Figure 4 harboring the indicated Hsp104 variants or empty vector control were induced in galactose media for 5 hours at 30°C. Yeast were lysed and the lysates were visualized via Western blot. PGK1 serves as a loading control.

Related to Figure 4.

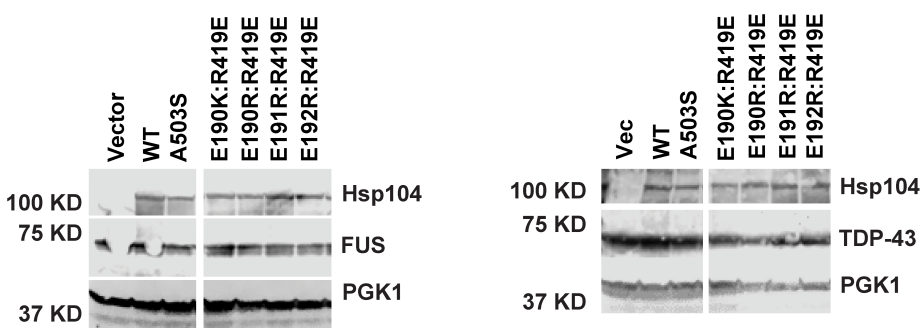


Figure S5. Western blots confirm Hsp104 variants and disease proteins are expressed at similar levels. Integrated $\Delta hsp104$ yeast strains from Figure 6C (left) and 6D (right) were induced for 5 hours in galactose media. Yeast were lysed and processed for western blot. PGK1 serves as a loading control.

Related to Figure 6.

	1. Ssa1 EC₅₀ (Figure 2B)	2. Sis1 EC₅₀ (Figure 2D, F)	3. Ydj1 EC₅₀ (Figure 2C, E)	4. Ydj1 IC₅₀ (Figure 2C, E)	5. Ydj1 IC₅₀ (Figure S2A)
Hsp104	~5μM	~2μM	~0.4μM	~14μM	~40μM
Hsp104^{R366E}	~6μM	~1.9μM	~0.047μM	~0.63μM	~20μM
Hsp104^{R419E}	~5μM	~3μM	~0.08μM	~1.3μM	~30μM
Hsp104^{A503S}	ND	~2μM	~0.21μM	~6μM	ND

Table S1. Summary of EC₅₀ and IC₅₀ values. From left to right: 1. EC₅₀ of Ssa1 for stimulation of luciferase disaggregation and reactivation by Hsp104 variants in the absence of Hsp40 (Figure 2B). 2. EC₅₀ of Sis1 for stimulation of luciferase disaggregation and reactivation by Hsp104 variants in the presence of Ssa1 (Figure 2D, F). 3. EC₅₀ of Ydj1 for stimulation of luciferase disaggregation and reactivation by Hsp104 variants in the presence of Ssa1 (Figure 2C, E). 4. IC₅₀ of Ydj1 for stimulation of luciferase disaggregation and reactivation by Hsp104 variants in the presence of Ssa1 (Figure 2C, E). 5. IC₅₀ of Ydj1 for dissociating β-casein from Hsp104 variants (Figure S2A).